

Aerosol Time-of-Flight Mass Spectrometry (ATOFMS) as a Real-Time Monitor of
Individual Aerosol Particles in Field Studies

Final Report
Contract 95-305

Prepared by Professor Kimberly A. Prather
Department of Chemistry
University of California, Riverside*

Prepared: March 1998
Final Edits: August, 2001

*Now at University of California, San Diego

Chapter 1

Introduction to aerosol time-of-flight mass spectrometry

Objective of Project: To develop transportable instruments which can be used to characterize the spatial and temporal variations of the size and chemical composition of individual airborne particles. Once developed and tested as part of this contract, these instruments will be used at various locations in the State of California to characterize aerosol sources and transformations as they occur in the atmosphere.

1.1 Motivation for performing single particle analysis

Recent developments of methods for the study of individual aerosols in real time present new opportunities for characterizing aerosol sources, transport processes, and transformations in the atmosphere. Information at the single particle level could potentially allow for source-specific regulation on particulate matter. Currently, particulate matter standards are the only ambient air quality regulations that are not chemically specific. Requirements of the PM_{2.5} and PM₁₀ standards may pose a number of problems in many regions of the United States. For example, in a number of areas it will be possible to exceed the mass-based particulate air quality standards based on particles produced by natural processes (i.e. sea spray, wind-blown dust). In such instances, regulating particles based on their chemical content or specific sources may be more desirable, given the possibility that the chemical speciation of particles may potentially pose a greater threat to human health than the total mass of PM for a given size fraction (Godleski 1998).

One significant difficulty involved in creating an effective PM standard involves the fact that not all PM is alike. In other words, when regulating ozone or NO_x species, these are well defined molecules and one ozone molecule is exactly the same as another. In contrast, one

particle does not necessarily resemble another particle chemically. How does one account for differences between particles to allow for control of the “right” particles or those that pose the greatest health threat? Our approach to this problem has been to develop a technique that characterizes each individual particle. This technique allows one to sort out one particle from another, thereby retaining its source identity as well as providing information on subsequent chemistry it may have undergone in the atmosphere. In contrast to filter sampling, there is little cost associated with continuously sampling particles for extended periods of time. Furthermore, information is obtained on the particles present in the atmosphere instantaneously, as opposed to waiting months for the analytical results to return from the lab. Because it is a real-time technique, ATOFMS data has the necessary temporal resolution (~10 minutes, see Chapter 6) to be correlated with other gas phase measurements, meteorological data, and air parcel trajectory information. Also, because particles are analyzed less than 1 millisecond from the time they are sampled from the air, very little alteration in size or composition occurs, allowing for the potential to analyze semi-volatile species including ammonium, nitrate, water, and semi-volatile organic species.

1.2 Aerosol time-of-flight mass spectrometry

While a great deal has been learned about atmospheric aerosols through the use of quantitative filter and impactor measurements, these techniques are limited for several inherent reasons discussed above. Our approach involves the technique, aerosol time-of-flight mass spectrometry (ATOFMS), which provides the size and chemical composition of individual particles in real-time. Complete details of the instruments are provided in Chapter 2, however a brief description of the operating principles of aerosol time-of-flight mass spectrometry are provided here. Air from the atmosphere is pulled directly into the vacuum of the instrument

through a converging nozzle. Each particle is accelerated through the nozzle, reaching a terminal velocity which is proportional to its aerodynamic size. Smaller particles reach a higher velocity than larger particles. In the sizing region of the instrument, the velocity of the particles is measured using two continuous wave diode-pumped Nd:YAG lasers operating at 532 nm (Brimrose Corp.). Particles scatter light as they pass through these two lasers separated by a distance of 6 cm. The measured time between these two scattering events is used to determine the velocity the particle is moving. The velocity can be used to obtain the aerodynamic size of the particle from a calibration curve created using particles of known size. Furthermore, the velocity can be used to time the arrival of the particle in the center of a time-of-flight mass spectrometer, where a Nd:YAG laser is fired at the appropriate time to desorb and ionize chemical species from the sized particle. The instrument is operated continuously, measuring the size distribution of the particles as well as correlated single particle chemical information.

In recent years, there have been a number of approaches aimed at characterizing individual particles (Johnston and Wexler 1995; Wood and Prather 1998). Most of these techniques use an optical method to detect the particles. Some of these methods correlate the intensity of light scattered by particles as they cross a laser beam to their size (Hinz, Kaufmann et al. 1994; Carson, Neubauer et al. 1995; Murphy and Thomson 1997). Others measure the flight time between two laser beams (Prather, Nordmeyer et al. 1994; Yang, Reilly et al. 1996) or between two focal points of one laser beam (Weiss, Verheijen et al. 1997). ATOFMS is unique from other single particle mass spectrometry instruments in that it can be used to analyze the aerodynamic size of all particles entering the instrument ($0.1 \mu\text{m} < d_a < 10 \mu\text{m}$). In contrast, other instruments that also aerodynamically size particles can only analyze one predefined size at a time and are forced to scan the size range of interest which has obvious limitations.

The ATOFMS approach of aerodynamically sizing particles from a polydisperse sample as they enter the instrument allows one to obtain compositionally-resolved size distributions (Noble and Prather 1996). An example of this is shown in Figure 1.1 where particles are divided into distinct chemical classes based on their mass spectra, organic, marine (sea salt), and soil. The most distinct thing to notice in these graphs is the break that occurs at approximately 1 μm . This break separates those particles that are generated by combustion processes (organic) from those that are created by mechanical processes (soil and sea salt). Because this is the size where we observe distinct compositional differences, we refer to fine particles as those $< 1 \mu\text{m}$ and coarse particles as those $> 1 \mu\text{m}$. In the South Coast Air Basin, this is consistently where the break between fine and coarse particles is observed from day to day by ATOFMS. As PM concentrations change, one can observe changes in the relative contributions from these two modes. During this time period, the PM_{2.5} mass concentrations was 23 $\mu\text{g}/\text{m}^3$, indicating a substantial number of fine ($<1 \mu\text{m}$) particles were present during this particular sampling period. At times, when the PM_{2.5} mass concentrations are higher, the coarse mode ($>1 \mu\text{m}$) counts dominate. These periods occur when there are high winds or air is being transported from the ocean. As shown in Figure 1.1, the current standard of PM_{2.5} clearly includes contributions from sea salt and soil. The relative position of this divide could cause future problems in certain regions of the U.S. where suspended dust or sea salt could lead to extremely high PM_{2.5} levels. One should note that although in Southern California the break between fine and coarse particles occurs at 1 μm , in humid environments, the break will occur at higher sizes. Measuring single particle size and composition distributions will assist in developing more appropriate cut point(s) in areas with differing climates and particle sources.

Obtaining data on individual particles provides unique information on particles that

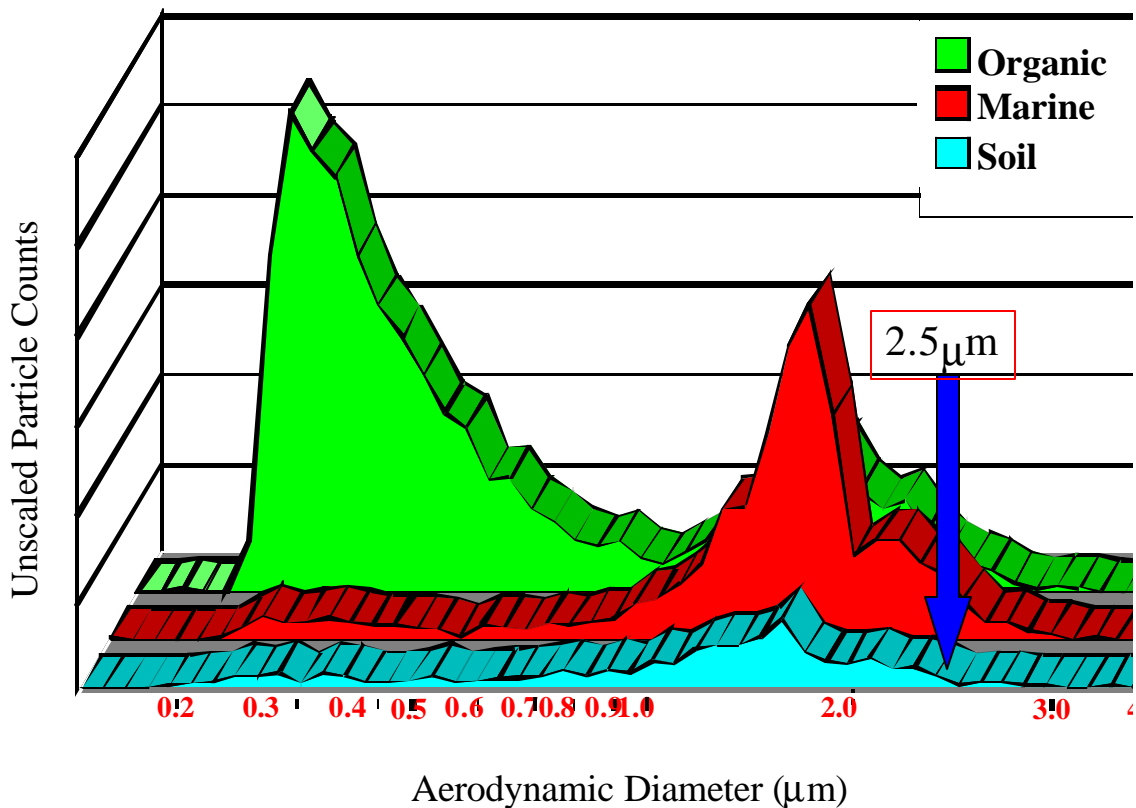


Figure 1.1 Compositionally resolved particle size distributions for particles sampled in Riverside, CA.

ultimately can be broken down into size/composition distributions as a function of source. This will be accomplished after completion of studies investigating particles directly from various sources which will allow us to obtain the individual signatures and size information that can be used to identify and track source-specific particles in the atmosphere (Liu, Rutherford et al. 1997; Silva and Prather 1997). Furthermore, using the relatively simplistic chemical classification scheme in Figure 1.1, we can use ATOFMS to monitor different particle types over time as shown in Figure 1.2. This figure can be obtained instantaneously in the field to determine which particle types are making the most significant contributions to the PM_{2.5}

fraction. It is important to note that the data shown in Figure 1.1 and 1.2 represent a very simplified chemical classification scheme. For example, once single particle source signatures are obtained, we will go a step further and sub-divide the organic particles further into classes based on sources (i.e. diesel vs. gasoline emissions). With this level of information, one could envision putting one ATOFMS instrument directly next to the source of interest and monitoring particles over time. Another ATOFMS instrument could be placed at various locations further from the source to characterize the evolution of these particles over time and distance. These are the types of field studies we plan to perform with the transportable ATOFMS instruments once they are completely characterized and optimized.

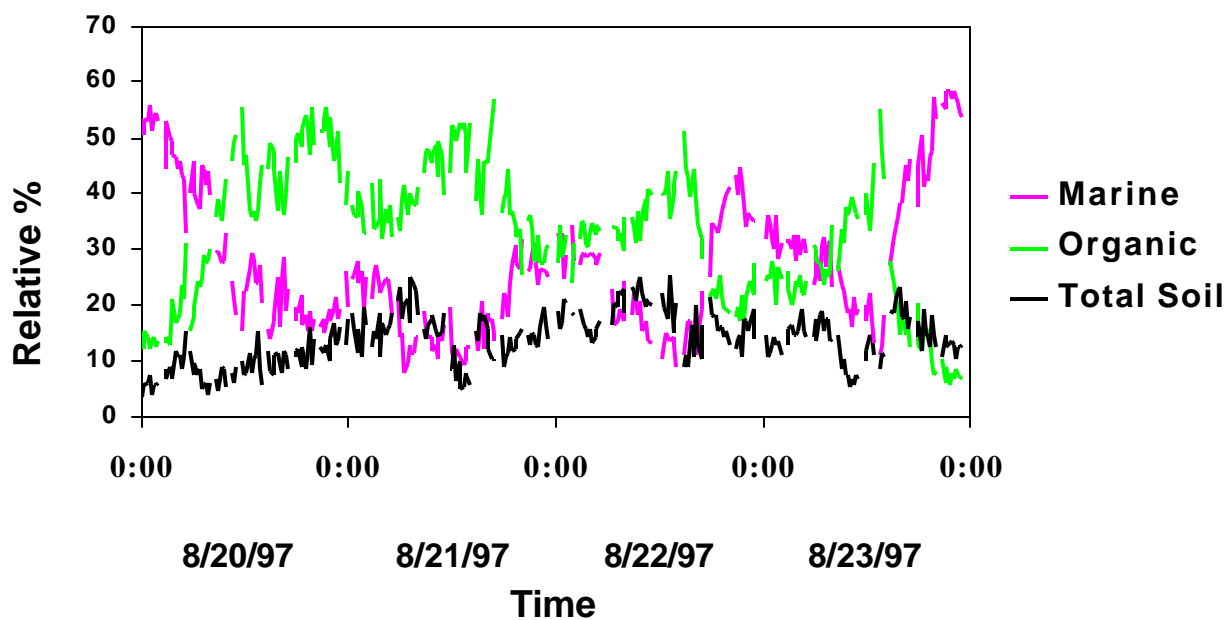


Figure 1.2: Temporal variations of particle classes over a 4 day period.

Chapter 2

Experimental description of transportable ATOFMS instruments

2.1 Overview

During the past decade, a number of researchers have been involved in the development of instruments which provide real-time information on aerosol particle composition in the atmosphere (Wood and Prather 1998). Over this time, we developed an aerosol analysis technique, aerosol time-of-flight mass spectrometry (ATOFMS), which is capable of simultaneously monitoring both the precise size and chemical composition of individual particles from a polydisperse aerosol in real time (Prather, Nordmeyer et al. 1994). A major shortcoming of real-time single particle mass spectrometry techniques has been their inability to routinely characterize the aerosol phase at more than a single geographic location, severely hindering their utility for atmospheric monitoring. Therefore, as part of this project, a new generation of transportable instruments were developed -which can provide insight into the geographic variations, transport characteristics, and chemical dynamics of atmospheric aerosols.

These two transportable aerosol time-of-flight mass spectrometers (ATOFMS) of identical design were constructed in the Chemistry Department at the University of California, Riverside (Gard, Mayer et al. 1997). Each is capable of analyzing the size and composition of individual particles from a polydisperse aerosol in real-time. Particles are introduced into the instrument using a particle beam interface, aerodynamically sized using the delay time between two scattering lasers, and compositionally analyzed with a dual polarity laser desorption ionization time-of-flight mass spectrometer (LDI-TOF-MS). The instruments measure 72" long x 28" wide x 60" high and weigh 500 lbs. Pneumatic tires allow the instruments to be moved

through standard doorways, elevators, and handicap ramps; granting access to virtually any location. Furthermore, because of rugged construction these instruments can operate while in motion during transport by automobile, boat, or aircraft. These instruments are powerful new tools for characterizing the origin, reactivity, and fate of atmospheric aerosols.

2.2 Operating principles of field transportable instruments

A schematic of the field transportable instrument is shown in Figure 2.1. Particles are

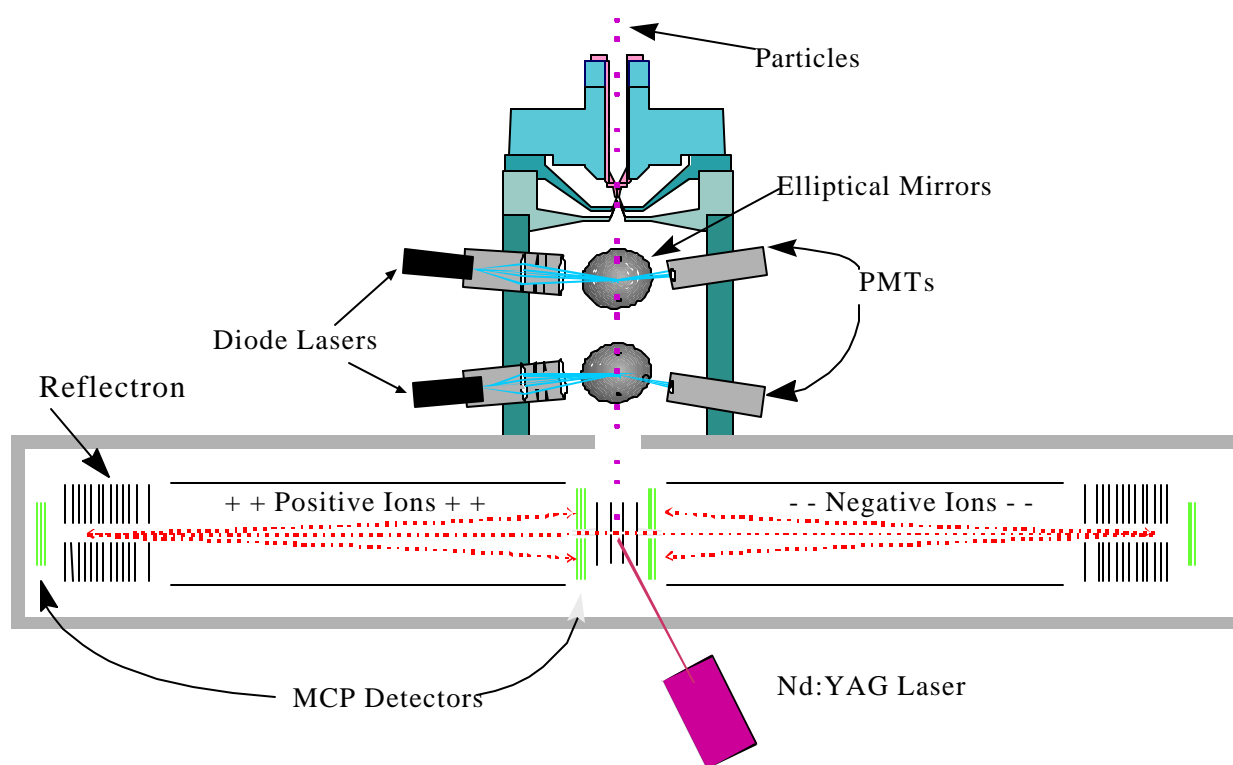


Figure 2.1: Schematic of field transportable instruments.

sampled from ambient atmospheric conditions into an aerosol beam interface as shown in Figure 2.1. The particles first encounter an inlet nozzle, which they enter at atmospheric pressure (760 Torr) and exit at 2 Torr. This pressure differential causes the gas to undergo a supersonic expansion during which small particles are accelerated to a higher terminal velocity than large

particles. This size dependent velocity distribution within the particle beam is the basis for determining the aerodynamic diameter of the particles in the particle sizing region of the instrument (Dahneke and Cheng 1979). After expansion through the nozzle, the aerosol beam passes through two stages of differential pumping before entering the particle sizing region.

Once in the sizing region, the particle passes through a continuous wave diode laser beam, generating a pulse of scattered light which is collected by a photomultiplier tube detector (PMT). After traveling 6.0 cm further through the interface, the particle encounters a second laser beam oriented orthogonally to the first, generating a second scatter pulse which is collected using an additional PMT. Thus, knowing the distance between the scattering lasers and the time between the two scatter pulses, the particles velocity is determined which upon instrument calibration can be used to obtain the particle's aerodynamic size.

The outputs of both PMTs are sent to a timing circuit, which is used to track the particles and control the firing of the Nd:YAG desorption/ionization laser. As the particle is being "tracked", it continues traveling through the scattering region and eventually enters the source region of a laser desorption ionization time-of-flight mass spectrometer (LDI-TOF-MS). When the particle reaches the center of the ion source, the timing circuit fires the desorption/ionization laser at the appropriate time to desorb and ionize material from the sized particle. The TOF-MS simultaneously monitors both the positive and negative ions generated by the desorption/ionization event.

Transportability features

Each of the two transportable instruments measures 72" long by 28" wide by 60" high and weighs approximately 500 pounds. To keep track of the instruments when referring to them, they were named in the order completed as "Jake" and "Elwood", respectively. An aluminum

framework supports the main body of the instrument and its ancillary components. Due to their weight, the three roughing pumps are mounted at the very bottom of the cart, keeping the center of gravity low to prevent the instruments from overturning. Additional components (diode lasers, Nd:YAG laser power supply, laser power meter, high voltage box, control box, vacuum gauge controller, and turbo pump controllers) are mounted toward the bottom of the aluminum framework, again to maintain a low center of gravity. The interface, particle sizing, and mass spectrometer units are located in the upper portion of the framework. Finally, the computer which controls all instrumental components is mounted above the main framework with the screen and keyboard at a convenient height for the operator.

For mobility, Jake and Elwood are fitted with pneumatic tires affording them access to most locations through the use of standard doorways, elevators, sidewalks, and handicap ramps. Additionally, for locations with difficult access, they were designed to be lifted by helicopter, crane, or forklift. However, the standard method for long distance transportation is to simply load them into a truck using a lift gate and secure them in place for the trip.

During the design phase, a great deal of thought was given to making each subsystem rugged enough for constant movement. In fact, in its initial field trip, our first transportable ATOFMS instrument was tuned-up in lab, unplugged, loaded into a truck, driven the 90 miles from Riverside to Long Beach, unloaded, powered-up, and hitting particles 10 minutes later with no tuning necessary, thereby proving our design efforts were effective. The specific steps taken to ensure this robustness are explained in the following sections.

Interface/Vacuum System

The interface region draws in air and entrains particles at a rate of $20 \text{ ml}\cdot\text{s}^{-1}$. This sampling rate is determined by the first conductance limit in the system, an inlet nozzle having

an initial diameter of 5.08 mm tapered at 30° to a final diameter of 0.342 mm; this diameter is maintained for a distance of 3.53 mm where the nozzle terminates. The region between the end of the nozzle and first skimmer is held at a pressure of 2 Torr by an 18 cfm mechanical pump (model E2M18, Edwards High Vacuum, Inc., Grand Island, NY). The first skimmer (Beam Dynamics Inc., Minneapolis, MN) has a 0.5 mm conductance-limiting orifice which is centered 2 mm beneath the exit of the nozzle. A second conductance limiting skimmer (also 0.5 mm diameter) is located 2 mm beneath the first. The stage between the two skimmers is maintained at 5×10^{-2} Torr by a second 18 cfm mechanical pump.

The sizing region, between the second skimmer and conductance limit to the mass spectrometer, is evacuated to a pressure of 5×10^{-5} Torr by a 70 l/s turbomolecular pump. A 0.3 x 3.0 cm conductance-limiting tube separates the particle sizing region from the time-of-flight mass spectrometer. The mass spectrometer region is evacuated to a pressure of 2.0×10^{-7} Torr by two 250 l/s turbomolecular pumps— one standard 250 l/s pump and one split flow 250 l/s (Varian). The low vacuum input of the split flow pump is used to back the standard 250 l/s pump as well as the 70 l/s pump on the scattering region. The split flow pump is, in turn, backed by a third 18 cfm mechanical pump.

Insuring accurate sizing and straight particle trajectories through the instrument requires that the inlet nozzle expansion conditions be very consistent. During sampling, however, the nozzle can slowly become restricted as particles accumulate and must be cleaned periodically (once every 2 to 4 hours during high particle fluxes). Therefore, we designed the particle interface with an interlocking ball valve to allow nozzle extraction and cleaning while the instrument remains under vacuum in standby mode. The whole process generally takes 3-5 minutes. In addition, to prevent excessive wear to the surfaces which keep the removable nozzle

aligned, an extraction mechanism was designed to minimize wear, prevent accidental venting, and avoid nozzle damage.

Manipulating the distances between the nozzle and skimmers provides control over the expansion conditions that accelerate the particles entering the instrument and can be adjusted to maximize particle focusing and transmission through the interface region. It is a unique feature of the ATOFMS instruments and is currently being used to study the effects of varying distances on particle transmission as a function of size. The upper stages of the instrument are adjustable and allow a minimum separation of 2 mm and a maximum separation of 9 mm between the nozzle and first skimmer as well as between the first and second skimmers. Changing the separation distance is accomplished by simply inserting flat shims between the stages, and is possible because of the gland seal o-rings used between each stage.

Being able to change distances between the nozzle and first skimmer and two skimmers is essential to optimizing particle transmission into the ATOFMS instrument for various size particles. In fact in studies conducted after the Fall 1996 study described in this report, we were able to dramatically improve our ability to detect submicron particles by changing these distances. Specifically, the distance between the nozzle and first skimmer was increased from 2 mm to 3.5 mm, and the distance between the two skimmers from 2 mm to 4.4 mm. This configuration allows us to efficiently transmit and detect particles from 0.08 to 2.5 μm , making our current portable instruments ideally suited for $\text{PM}_{2.5}$ characterization.

To preserve alignment during movement and assembly, each interface stage is designed to key into the subsequent stage. In addition, the removable nozzle has a close fitting Teflon bushing which allows it to move and simultaneously preserves alignment. Each skimmer keys into a recess which is concentric with the outer alignment diameter of the stage. The last stage of

the interface keys into the body of the sizing region which, in turn, keys into the mass spectrometer region thereby maintaining alignment throughout the instrument to well within 0.008 mm. Furthermore, each of the three interface stages was machined from a solid piece of T-6061 aluminum to minimize weight, machining time, and to eliminate the need for welds. The vacuum seals are made by o-rings that seal on the diameter of each stage as opposed to face seals, which helps eliminate misalignment between stages and allows skimmer/nozzle distances to be adjusted easily.

Pressure measurement is accomplished using a vacuum gauge controller (HPS, Boulder, CO) with Pirani gauges on the first two stages and cold cathode gauges on both the light scattering and mass spectrometer regions. The cold cathode gauges were selected over ionization gauges for their durability. The gauge controller has a safety interlock system which shuts off the high voltage when the pressure exceeds a preset threshold value. This prevents arcing in the event of an unexpected vacuum loss.

Because of the high load placed on the pumps, particularly the first one, all mechanical pumps are fitted with oil mist filters and oil return systems to prevent generation of oil mist particles. In addition, to eliminate potential oil back streaming into the interface, all mechanical pumps are equipped with in-line oil traps. The turbo pumps are air cooled which eliminates the need for a bulky water cooling system. They can also be operated in any orientation, placing no restrictions on the orientation of the instrument.

In an effort to make the pumping system more robust, some redundancy was designed into the system in that, should any one turbo or mechanical pump fail, the others can be rerouted to evacuate the system with a pump-down time of 30 minutes instead of the usual 10 minutes. This robustness is an essential feature when operating the instruments for extended periods in

remote locations.

Aerodynamic Particle Sizing Region

This is the region of the instrument that makes ATOFMS unique from other real time particle mass spectrometry instruments. The ability to simultaneously characterize both the size and composition of each individual particle was developed in our lab (Prather, Nordmeyer et al. 1994).

Once the particles have passed through the particle interface, they enter the sizing region (shown in Figure 2.1) where aerodynamic sizing takes place. The particles pass through two continuous-wave laser beams. The two scattering signals are detected and sent to a timing circuit which both records the transit time of the particle between the two lasers and prepares a Nd:YAG laser to perform desorption/ionization of the sized particle.

In the initial phase of development of the two portable instruments, fiber optics were used to send the laser beams in from an argon ion laser. This eliminates the need to align the bulky argon ion laser itself, making it possible to simply rack mount the laser and only worry about aligning the fiber optic output. Therefore, the argon ion laser (Omnichrome, Model 532, 220 Volt) is coupled onto the input side of a 100 μm multimode fiber optic power splitter (AMP Corporation, Model 2-107842-1). Each output fiber is inserted into an assembly that contains a collimating/focusing lens which brings the beam to 1 mm spot size. In addition, extensive iris-ing is employed to control stray radiation. This assembly is placed into an XZ translator (Thor Labs, Newton, NJ) which is then adjusted to optimize the light scattering intensity. The entire beam probe assembly is modular and easily removed from the main body for maintenance or modification. The laser beam is terminated by a custom made light horn, a device that efficiently scavenges excess scattered light in the system, thereby minimizing background signal from stray

light. For durability in the field, the light horns which scavenge stray radiation are made of copper instead of glass, which is typically used in the laboratory. This optical arrangement retains alignment under normal transportation conditions and even when substantial shocks are encountered. If alignment is lost, the system has proven easy to realign.

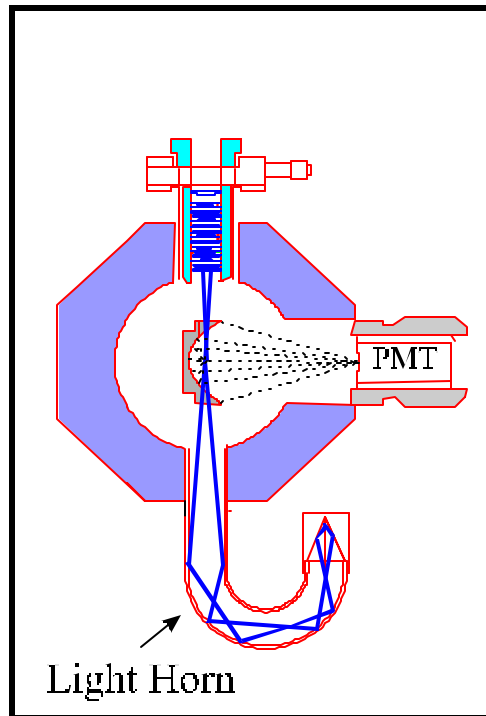


Figure 2.2: Cross sectional view of light scattering region in transportable instruments.

As shown in Figure 2.2 above, to maximize light collection efficiency, each scattering laser beam intersects the particles at one focus of an elliptical mirror such that, when a particle intersects the laser beam, the resultant scattered light is concentrated at the other focus of the ellipse. The light pulse is detected by a PMT placed directly at the second focal point. Each elliptical mirror and PMT pair is held in a precision made module to maintain proper spatial and angular orientation with respect to the particle beam. The mirror/PMT module is easily removed from the main body of the scattering region for cleaning and maintenance.

The configuration described above was used for initial experiments described in this

report. The smallest particle that could be detected was 0.2 μm in diameter. Given the expansion conditions of the instrument as determined by the nozzle, the largest particles we typically observe in ambient sampling range from 3-7 μm . At typical ambient concentrations, our size distribution typically tails off at 3 μm ; at high concentrations resulting from conditions such as high winds, we observe particles up to 7-8 μm .

Just as in the interface, the main body of the sizing region and its supporting components are made, primarily, from aluminum to minimize weight and machining time. Additionally, the main body of the scattering region was machined from a single piece to retain alignment and all vacuum seals are made with Viton o-rings to simplify assembly and disassembly procedures.

In the past six months, we have replaced the Ar ion laser with diode pumped Nd:YAG lasers (as indicated in Figure 2.1). These consume much less power, a major consideration for field deployment. In addition, they can be focussed more tightly, providing an increased in the power density from 57 mW/mm^2 to 121 mW/mm^2 . This increase has extended the lower particle size detection limit to 0.08 μm (Gaelli, 2001). Furthermore, the diode lasers are mounted directly to the body of the particle sizing region of the instrument, adding to the ruggedness and stability of the instrument.

Timing Circuit

The timing circuit in the field portable ATOFMS is crucial for obtaining both particle velocity, which is related to aerodynamic diameter, as well as ensuring that the sized particle is desorbed and ionized by the Nd:YAG laser. A block diagram of the function of the timing circuit is shown in Figure 2.3.

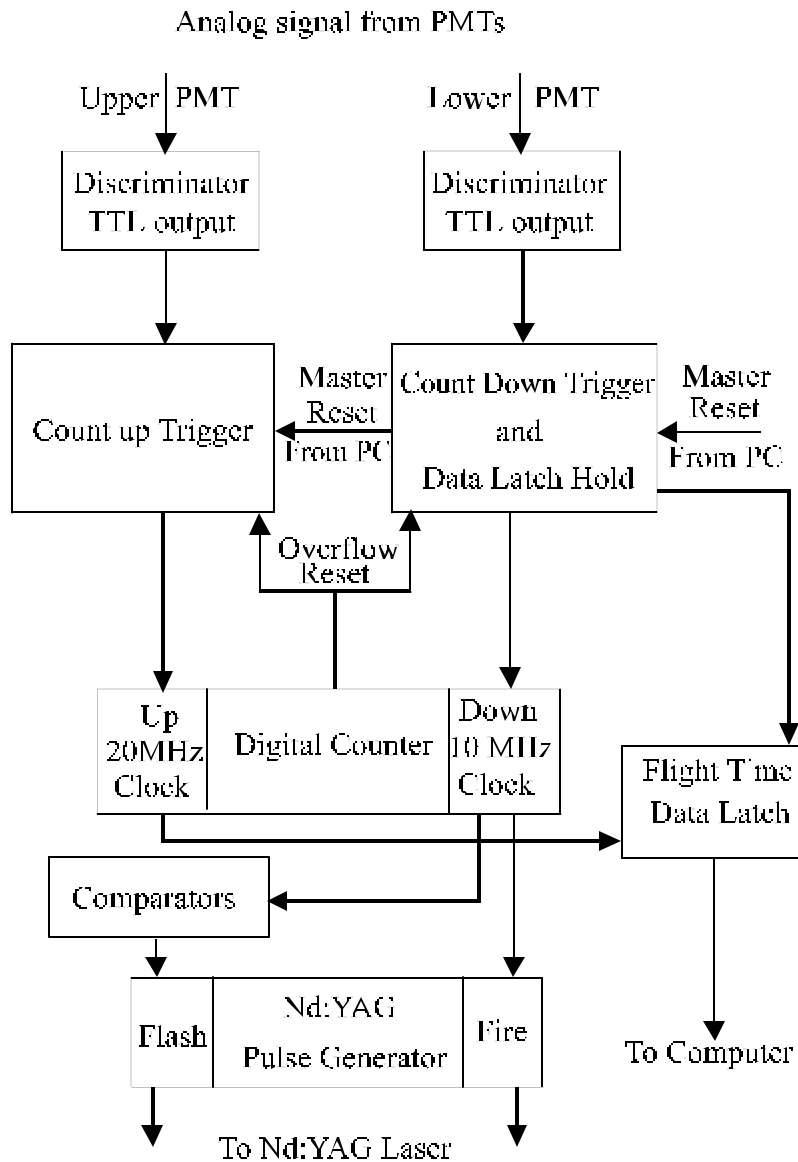


Figure 2.3: Block diagram of functioning of timing circuit.

The light scattering signal first enters the timing circuit as an analog pulse from the upper PMT in the particle sizing region and is converted by a discriminator to a TTL pulse. This pulse starts a 16 bit digital counter running at 20 MHz. Concurrently, the count-up trigger locks out other TTL pulses until it is reset, either by reaching a maximum value corresponding to 800 μ s (overflow reset) or by completing a “track & fire” sequence (master reset from the computer), to prevent a “double-trigger”.

The signal from the second PMT starts a counter operating at 10 MHz and signals the flight time data latch to hold the value of the counter. The slower count-down rate (10 vs. 20 MHz) accommodates the 1:2 distance ratio between the two light scattering lasers (6.0 cm) and the distance between the second scattering laser and the center of the mass spectrometer source (12.0 cm). This additional distance is required because of the warning/firing time needed for the Nd:YAG laser ($200 \pm 5 \mu\text{s}$).

When the counter reaches +200 μs and 0, a trigger pulse is sent to the Nd:YAG flash lamps and a fire pulse is sent to the Q-switch of the Nd:YAG, respectively. Once the Nd:YAG laser has fired, the computer reads the flight time data latch, acquires the mass spectrum, and sends the master reset signal to prepare the timing circuit for the next “track and fire” event.

Mass Spectrometer Design

The time-of-flight mass spectrometer is designed to analyze both positive and negative ions generated by the desorption/ionization of a particle. A reflectron design was used because of its ability to enhance spectral resolution by compensating for the ion kinetic energy distribution that results from the laser desorption/ionization process (Mamyrin 1994). Furthermore, a coaxial design was selected to minimize size and complexity.

The dual-ion coaxial reflectron mass spectrometer requires that the two primary detectors be mounted back to back close to the source region and possess center holes for the ions to pass through as they exit the source, as seen in Figure 2.1. Initially in the instruments, the primary detectors were 70 mm diameter MicroSphere Plates (MSP) (El-mul Technologies Yavne, Israel), with a 6 mm center hole and a flat anode. Due to instability of the MSP detectors, we replaced them with 40 mm microchannel plate (MCP) (Gallileo, Mass.) detectors. For the field study discussed in this report, MSP detectors were used.

Since they must possess holes in the center for the ions to pass through, the detectors require a flat anode instead of an impedance matched conical anode. When designing the instruments, there was some uncertainty as to whether this would be a potential cause of signal distortion. However, no such distortion was evident in the initial mass spectra. There was also concern that the ions might return back through the center of the detectors. Therefore to control the angular direction of the ion trajectories, the reflectrons are externally adjustable over a range of 2° , thus preventing such an occurrence. In addition to the primary detectors, each instrument also contains two 18 mm diameter MCPs with flat anodes behind the reflectrons. These may be used to detect ions in linear mode as a backup to the primary detector, for diagnostic purposes, or to detect the loss of neutral species.

In order to analyze both positive and negative ions, the two flight tubes and primary detectors are floated at high voltages. The instrument was designed to have one flight tube at +10 kV and the other at -10 kV. The ions are generated exactly halfway between the central source plates which are 10 mm apart, one is held at +5 kV and the other at -5 kV. After passing through the central hole in these first source plates the ions encounter a second source plate located 5 mm outside the first and held at +10 or -10 kV respectively. The detectors are also floated at high voltage to maintain a field free region and are capacitively decoupled from the data acquisition electronics by a circuit.

During the design phase of the dual polarity TOF-MS the ion optics were simulated using MacSimion 2.0 (Don McGilvery and Richard Morrison, Dept. of Chemistry, Monash University) on a Macintosh computer; an ion trajectory simulation, equipotential lines, and typical voltages are shown in figure 7. Electrode geometry was fine tuned to maximize resolution using the Simretof program (Dr. Gary Kinsel, University of Texas, Arlington) operating on a PC. The

actual resolution of the instruments when analyzing particles is typically 600 at m/z 165.

For particle desorption/ionization, a Nd:YAG laser (Minilight 10, Continuum, Santa Clara, CA) was chosen which when operating at 266 nm has a 5 ns pulse width and 1.0 mJ per pulse. When focused to a 500 μm spot size this generates a power density of approximately $1 \times 10^8 \text{ w/cm}^2$.

To enhance the field maintainability and ruggedness of the mass spectrometer, no grids were used in any of the plates in the time-of-flight mass spectrometer, as they are prone to being damaged even under lab conditions. Modified automotive spark plugs were used as high vacuum electrical feedthroughs because they work well, are inexpensive, and readily available. A plastic material (Kel-F[®]) holds and insulates all internal parts of the mass spectrometer instead of the ceramic (Macor[®] or alumina) which is typically used. This was done primarily because Kel-F[®] is resistant to inertial shock (it will not crack like ceramics) and is much easier to machine. To greatly increase the speed of and simplify assembly/disassembly procedures, the coffin chamber is sealed entirely with Viton o-rings. Furthermore, to modify or inspect any part of the mass spectrometer, one only needs to remove the chamber lid which grants access to all electrical and mechanical components of the mass spectrometer. The source, flight tubes, reflectrons, and detectors are secured in place with a total of six fasteners, and all electrical connections are made with quick disconnect in-line connectors making all the components easily accessed and removed. Once the fasteners and electrical connections are removed, the flight tubes and reflectrons can be removed entirely. In addition, the source and detectors are all mounted in a single cassette fastened to one of the flight tubes for ease of installation and removal.

The coffin chamber that contains the mass spectrometer components was designed to be

rectangular for several reasons. First, the flat surfaces on the exterior allow the ionization laser and associated optics to be mounted directly to the side of the chamber, thus minimizing the loss of laser alignment during transportation. Secondly, the square exterior makes it easy to mount the electrical feedthroughs, pressure gauge, and vacuum pumps directly on the chamber. The traditional round exterior, in contrast, makes it very difficult to mount electrical, pumping, and laser components anywhere but the end flanges of the chamber. The rectangular chamber was manufactured by hollowing out a 6" x 6" x 64" piece of 6061-T6 aluminum solid bar stock to have internal dimensions of 5" x 5" x 63" which accommodates the mass spectrometer components.

The twenty-one plates for each reflectron are made of 304 stainless steel and connected in series with 10 M Ω vacuum compatible resistors. The steel discs are held rigidly with four Kel-F rods and slipped into an aluminum canister to make a complete reflectron assembly. In addition, the source plates and flight tubes are also made of 304 stainless steel. Because of the different materials used in the instruments and the daily temperature variations they will experience, the design accommodates the different thermal expansion coefficients of the materials, thus preventing damage by thermal expansion/contraction in the field.

Data acquisition and control software

The data acquisition and control software was written in-house using Microsoft Visual Basic 4.0 running under Windows 95 on a Pentium-90 computer to control the components of the instrument, data acquisition, and data storage. The overall control scheme is depicted in Figure 2.4. The program interfaces with the instrument using TTL signals from an I/O board which are used to send/receive information from the timing circuit and are also used by the control unit to activate/deactivate specific instrument components. By this means, the program

orchestrates the start-up and shut-down sequences for all components of the instrument and can place the instrument in “idle” and “ready” modes in which unnecessary components (such as the lasers, PMTs, and high voltage) are turned off or set to low-power modes when data are not being acquired.

Each time the system goes through a “track and fire” sequence, the acquisition software: (1) reads the count number from the timing circuit and calculates the velocity of the particle, (2) reads the laser power from the laser power meter via an IEEE-488 bus, (3) reads the positive and negative ion spectra from the data acquisition boards, and (4) examines the acquired data to determine if the particle was hit or missed. Particles are considered hit when they produce a size and mass spectrum and missed when only a size is acquired. Due to divergence of the particle beam after the sizing region, typically between 10 and 30% of the particles are hit. If the particle was hit, the spectra and associated data (velocity, laser power, date/time, operating conditions) are saved in a hit-particle file. If, on the other hand, the particle was missed, no mass spectrum is acquired but the other data (velocity, date/time, operating conditions) are stored in a missed-particle data file. Based on this information, the program generates a real-time display containing either the real-time mass spectra from the particles or particle size histograms for both hit and missed particles as they are acquired. The program also displays the current operating conditions of the instrument, including the vacuum gauge readings and the status of each component of the instrument. When aligning the lasers, the instrument is “tuned” to hit particles over the entire size range by optimizing the correlation between the hit and missed histograms. The instrument is considered optimized when the overall shapes of the hit and missed particle size distributions are the same and there is no size biasing due to misalignment.

With the current hardware and software combination, the instrument can execute an

entire “track and fire” sequence in less than 100 ms if the particle is missed, and approximately 300 ms if the particle is hit. The 200 ms time difference is due to the time it takes to compress and store the spectra. Therefore, computer processing time limits the maximum “track and fire” rate to slightly less than the 10 Hz maximum repetition rate of the Nd:YAG laser. The firing rate is typically 6-8 Hz if particles are abundant. The tracking rate of the ATOFMS instrument is quite complex and depends on the atmospheric size distributions and relative particle counts. Both of these affect the rate the instrument can save data as well as the logistics of the timing circuit. We are currently investigating the dynamic range of the ATOFMS instruments by performing lab studies using controlled concentrations of particles of differing sizes.

Electrical systems

All of the pumps, lasers, power supplies, and other electrical devices on the instrument are under software control by an I/O interface (Keithley-Metrabyte PIO-96) connected to a custom built control unit (Figure 2.4). The control unit contains solid state relays to separately switch on and off the roughing pumps, lasers, vacuum and laser power meters, and power to the turbo pump controllers and high voltage power supplies. It serves as a power distribution center for the entire instrument (using inputs of 30 Amps at 110V and 220V) and provides circuit-breaker protection before it is switched and connected to each of the other components. The input power can be supplied by tapping an existing power grid or, in remote locations, by natural gas powered generators that we have procured for this purpose.

The control unit also contains the timing circuit which controls the firing of the Nd:YAG laser, a power supply, a control interface for the PMTs, and an interlock circuit which shuts off the high voltage power supplies if the pressure in the mass spectrometer exceeds a preset threshold. Separate control wires are connected through the control box to both lasers, the turbo

pump controllers, the high voltage power supplies, the vacuum gauge controller, and a solenoid valve which is used to vent the vacuum chamber via the rough pumps with dry nitrogen.

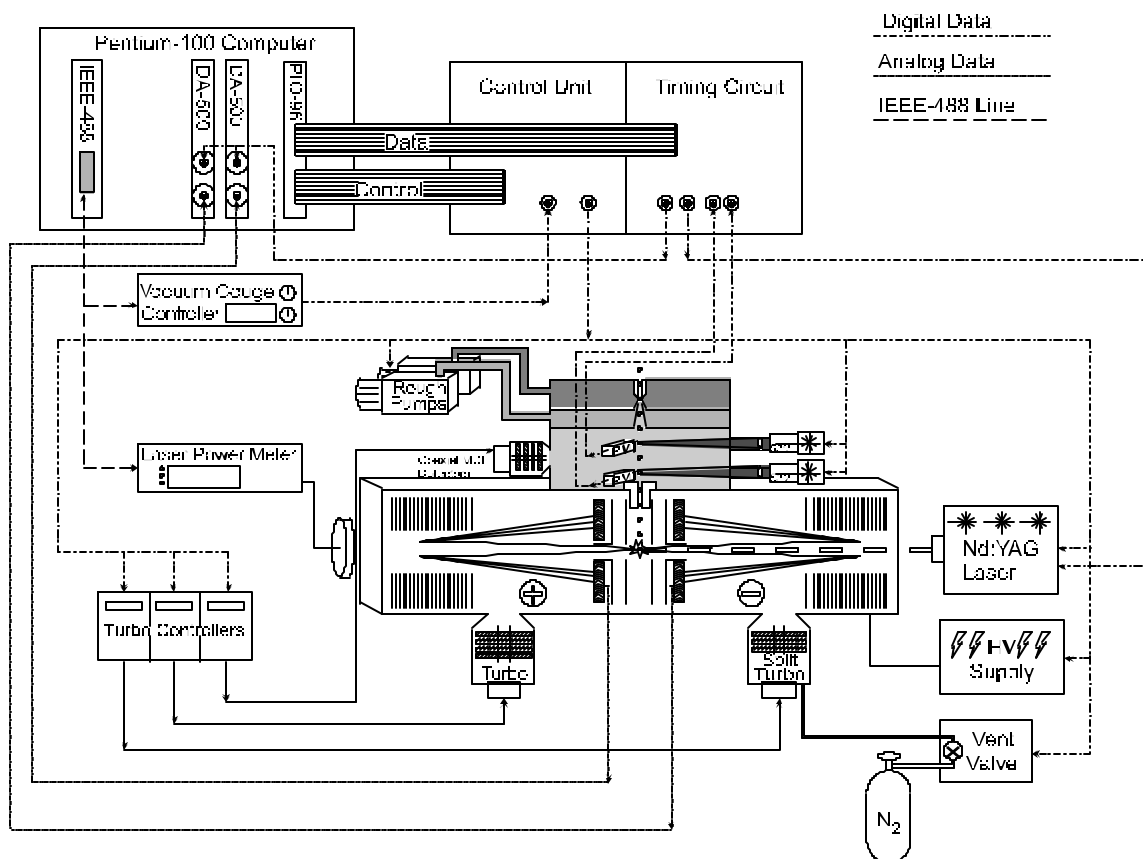


Figure 2.4: Schematic of control for timing for ATOFMS.

High voltage is provided by six negative and six positive voltage Spelman MP-15 zero to 15,000V adjustable power supplies which are built into a compact box with a low voltage power supply, adjustment controls, a voltmeter, and output connectors.

Frame construction

The frame, to which the main body of the instrument and all its components are mounted, is constructed from an extruded aluminum assembly kit (80/20 Inc., Columbia City, In). The kit was selected for its flexibility, ease of assembly, and light weight. The supporting electronics and

lasers are mounted on three standard 19" rack mounts that were bolted directly to the frame. The entire interface, light scattering, and mass spectrometer assembly is mechanically separated from the aluminum support structure by four rubber shock mounts to dampen vibration while in motion. In addition, the assembly has two pivot points located on the ends of the rectangular chamber. This allows the instruments to be used in virtually any position to accommodate any source from which we need to measure particles. This same feature allows the coffin chamber to be flipped on its side to remove the cover which vastly simplifies maintenance in the mass spectrometer region. Furthermore, both pivots have rubber shock mounts which further isolate the mass spectrometer from vibration.

2.3 Instrument optimization, calibration, and performance

Size calibration of instruments and lower size limit of particle detection

For size calibration of the instruments, particles of known size are sent into the ATOFMS instruments. Polystyrene latex spheres (PSL) are suspended in water and atomized using a home-built Collison atomizer. The sheath air is dried by passing it through a 25 cm long silica-gel filled drying tube and then a HEPA tube to remove contaminant particles. Eleven sizes of PSL's ranging from 80 to 2400 nm are used to calibrate the instruments. All calibration particles are dried using two 30 cm long diffusion driers filled with silica gel and then transferred to the inlet of the instrument through a Teflon tube. Between each run with different PSL's, the atomizer is rinsed with Milli-Q water, and pure water and atomized into the instrument. This is done to be sure that no particles are detected over a 10 minute interval, ensuring that the particles observed during the sizing experiment are indeed those put into and suspended by the atomizer.

In order to eliminate the possibility of contaminants in the Milli-Q water condensing onto the PSL's and increasing and thus changing the calibration particle's size, several sizes of PSL's are sampled out of a differential mobility analyzer (DMA) after being nebulized and dried as described above. The aerosol flowrate in the DMA is 1.2 L/min and the sheath flow rate is set to 3 L/min. The particles are transported directly from the output of the DMA into the ATOFMS. The corresponding particle velocities for particles sized with the DMA and for direct sampling from the atomizer are below shown in Table 2.1.

Size (μm)	Velocity (m/s) (\pm One Std. Deviation) Without DMA	Velocity (m/s) (\pm One Std. Deviation) Without DMA
0.080	496 (± 10)	507 (± 9)
0.098	499 (± 11)	506 (± 7)
0.140	499 (± 11)	507 (± 29)
0.220	491 (± 4)	498 (± 6)
0.304	468 (± 2)	
0.503	425 (± 3)	
0.701	405 (± 2)	
0.895	382 (± 1)	
1.24	354 (± 1)	
2.04	310 (± 1)	
2.40	290 (± 2)	

Table 2.1: Velocities and standard deviations for PSL particles used for size calibration curve.

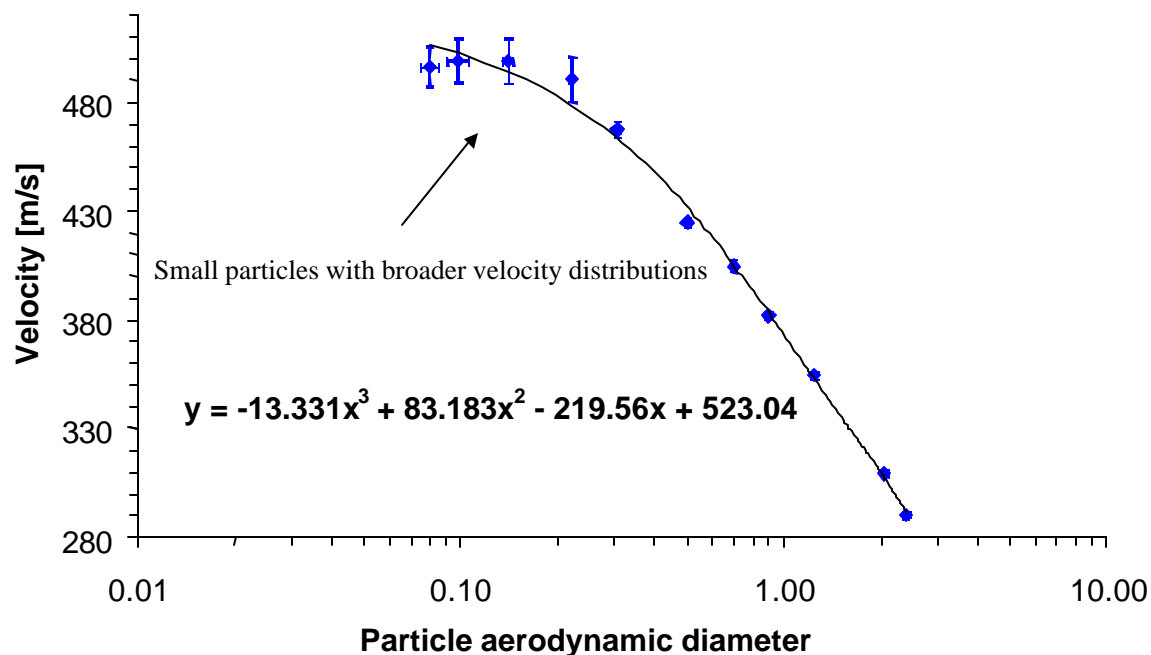


Figure 2.5: Calibration curve for transportable instrument.

Figure 2.5 shows the calibration curve obtained for PSL particles listed in Table 2.1, ranging in size from 0.08-2.40 μm. This graph illustrates the ability of the transportable ATOFMS instruments to detect particles as small as 80 nm in diameter. For each of the PSL sizes, the velocities of between 200 and 1300 were averaged. A third order polynomial fit was applied to these points, weighted to the inverse of the standard deviation of the measured velocity. As shown in Figure 2.5, this order fit was chosen because it gives the best fit ($R^2 = 0.994$) to the data down to approximately 0.2 μm. This is the range used for field studies with the ATOFMS instruments. The equation for the fit is given in Figure 2.5.

The difference in velocity of the particles with aerodynamic diameters of less than 220 nm is smaller than the standard deviation of the measured velocities. Thus, while precise size can not be determined for these particles, they can be optically detected, chemically analyzed, and sized as “smaller than 220 nm”. There are two possible explanations for the similarity in

particle velocities for the smallest PSL particles. First, smaller particles could be growing by condensation as they are introduced into the instrument. In order to minimize this possibility, the PSL's are run through a diffusion drier and then sent directly to the instrument without addition of room air. This possibility was investigated by sampling particles that were first sent through a DMA. PSL's were nebulized using a Collision atomizer, dried as described above and then transported into the DMA. By selecting the appropriate DMA voltages, only particles of the nominal size passed through the DMA and entered the ATOFMS. The velocities of these particles were compared to the velocities of particles sampled without putting the DMA first. As shown in Table 2.1, no significant increase in size (decrease in velocity) was observed for particles between 80 and 220 nm with or without the use of the DMA.

A second possible explanation for the observed spread in velocities for particles less than or equal to 140 nm is that these small particles are going very nearly the gas velocity (calculated by extrapolation to be 525 m/s), and therefore exhibit only very small changes in their measured velocity. At the same time, the standard deviation calculated for the velocity of the particles increases from 1-2% to approximately 10% for particles of 140 nm aerodynamic diameter and smaller. This corresponds to the velocity distribution of the gas molecules for an expansion at these conditions. Furthermore, the Stokes numbers decrease as the aerodynamic diameter of the particle decreases, thus causing the smaller particles to closely follow the flow of the expanding air.

The velocity of particles and the point at which the velocities of particles with different sizes can no longer be differentiated depends strongly on the nozzle design in the instrument, especially the diameter and length of the channel. By changing these parameters, the lower detectable size limit and transmission efficiency can be adjusted which allows one to increase the

resolution at the lower size end at the cost of a lower transmission efficiency for larger (supermicron) particles.

The two transportable instruments were constructed to be as “identical” as possible. Figure 2.6 shows a comparison of the size calibration curves for the two transportable instruments, showing how close they are to one another. This comparison shows the similarity of the instruments in the interface and light scattering regions, thus providing similar transmission and expansion conditions and allowing for direct comparison of the results obtained in field studies acquired at the same time at different locations.

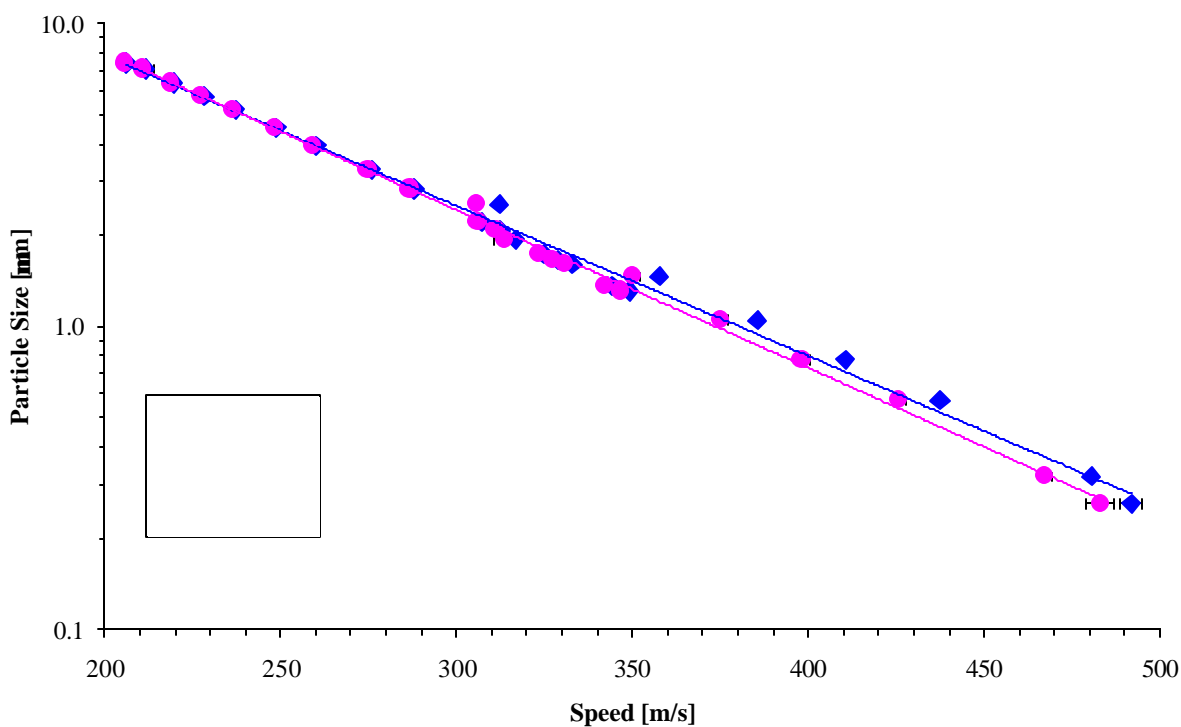


Figure 2.6: Comparison of initial size calibration curves for the two field transportable ATOFMS instruments.

Dual-Ion Mass Spectrometers

A unique feature of the portable instruments is the ability to obtain both positive and

negative ion mass spectra of individual particles. In a typical time-of-flight mass spectrometer, one can only obtain either the positive or negative ion mass spectrum of each particle. This provides limited chemical information. Different chemical species will produce positive or negative ions. For example, cations such as ammonium, sodium, metals, and organic species will form positive ions. Species with high electron affinities such as chlorine, bromine, organic acids, nitrate, and sulfate will form negative ions. Therefore dual ion information is highly complementary as shown in Figure 2.7 below.

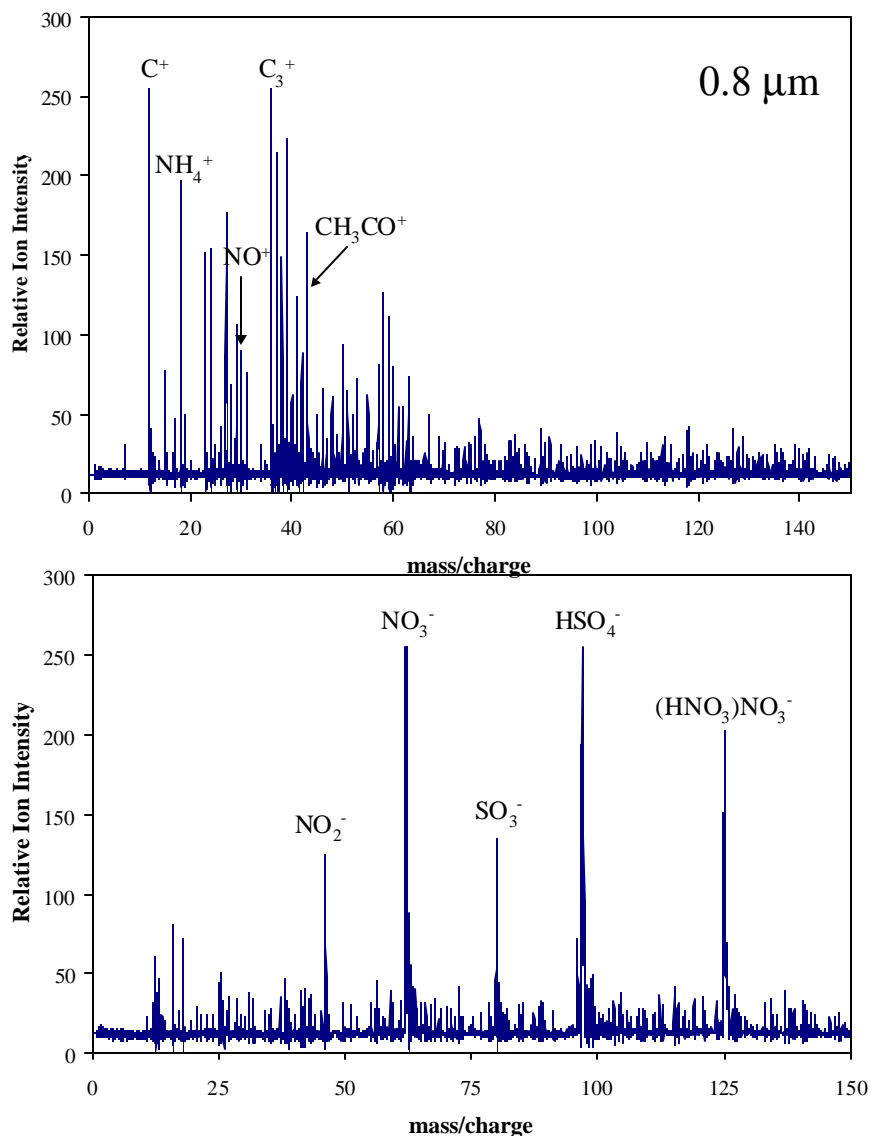


Figure 2.7: Positive and negative ion mass spectra produced by laser desorption/ionization of a single particle obtained with ATOFMS dual ion mass spectrometer.

As shown in Figure 2.7, the positive ion spectrum provides information on the organic species present in the particle, as well as the presence of ammonium and nitrate. In contrast, the negative ion spectrum provides information on the presence of nitrate and sulfate in the particle. It is important that we acquire as much chemical information on each particle as possible since we only get one shot at it.

The ability to measure both positive and negative ions is crucial to being able to

accurately identify sources. Often times, the positive or negative ion mass spectrum for particles from one source looks identical to those from another one, making source identification impossible. However, the combination of both positive and negative ion spectra is typically unique to a particular source, making the outlook for future source allocation using ATOFMS a promising one.

Chapter 3

Field Study Results

3.1 Overview of trajectory study conducted in Fall, 1996 in Long Beach, Fullerton, and Riverside, CA

Once constructed and tested, the transportable instruments were used in a field study in Fall of 1996 conducted in Southern California designed to a) study the aerosol chemistry that occurs in an air mass as it moves inland from the ocean through a polluted environment into Riverside, California, and b) calibrate the instruments alongside known aerosol measurement equipment.

The three ATOFMS instruments were calibrated against size-segregated, chemically speciated aerosol samples collected by inertial impaction. In addition, electronic particle size monitors, electrical aerosol analyzers, and optical particle counters were operated in parallel with the impactors to calibrate the ATOFMS particle sizing capabilities as well as confirm the mass distributions by comparison with the impactor samples. An overview of the experiment has been described by Hughes (Hughes, Allen et al. 1999, Hughes, et al. 2000). On the basis of weather predictions indicating probable inland air transport, four days (September 23 and 24 and October 1 and 2, 1996) were chosen for more extensive sampling. Intensive experiments were conducted over pairs of consecutive days to accommodate the previously observed travel time of air parcels across the basin (Russell, McRae et al. 1983). Three air monitoring stations were established during late September and early October of 1996 along a typical air parcel pathway crossing the Los Angeles Air Basin. Two additional days (September 25 and 26, 1996) were chosen for intensive sampling in Riverside only, because conditions there were very hazy and nitrate concentrations were observed to be particularly high on those days as determined by real-time sampling with the lab-based ATOFMS instrument. As shown in Figure 3.1, the chosen sites

were Long Beach, Fullerton, and Riverside.

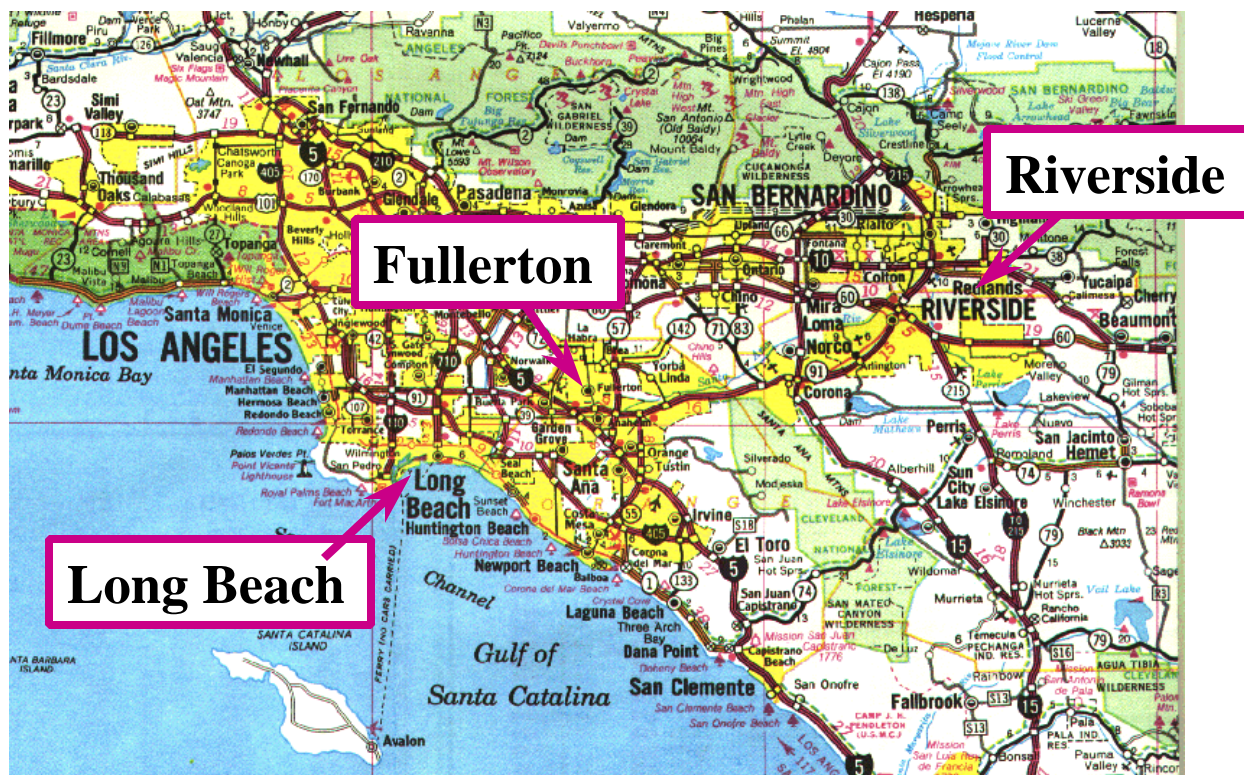


Figure 3.1: Map showing locations of three sampling sites in Long Beach, Fullerton, and Riverside used for field study.

The experiment was designed to permit a subsequent search for “single air parcels” that pass consecutively over several air monitoring sites as they are transported across the basin. Previous experience with experiments designed to achieve this objective suggest the following time scale is appropriate for this study: intensive sampling in Long Beach at 0700-1100 PDT, Fullerton at 1100-1500 PDT, and Riverside at 1500-1900 PDT. During these times, the chemical composition of the particles was measured as a function of size on samples collected for 4 hours with micro-orifice impactors (MOUDI’s) at each site.

By combining the September 21-22 background measurements at Santa Catalina Island with the September 23-24 intensive experiments and the September 25-26 experiments at Riverside, a 5-6 day consecutive period of observations exists as air parcels are advected across

the air basin. Data for the trajectory portion of this study are still being compared and analyzed.

Particles were sampled continuously with ATOFMS over a two week period in Riverside, CA and Long Beach, CA from 9/23/96 through 10/2/96 with breaks in sampling for cleaning the nozzle inlet to the ATOFMS. ATOFMS data were also collected in Fullerton on October 1-2, 1996 from 1100-1500 PST. Impactors were run in Riverside during six intensive periods on 9/23/96-9/26/96 and 10/1/96-10/2/96 for four hours each day from 15:00-19:00 PST for a total of 24 hours of particle sampling. Impactors in Long Beach were run on 9/23/96-9/24/96 and 10/1/96-10/2/96 for four hours each day from 8:00-11:00 PST. These dates and times were chosen on the basis of meteorological predictions which indicated probable air transport along the set pathway.

3.3 Results from peripheral instrumentation (Caltech Group)

The sizing instruments and off-line chemical analysis samplers were operated by Professor Glen Cass's research group. The results from their analyses are summarized in Table 3.1. The results reported in this final report focus on the ATOFMS results. For further information on the CIT results, the reader is encouraged to read two references detailing the study (Hughes, L., et al. 1999 and Hughes, L. et al. 2000).

	Long Beach			Riverside		
	mean	range		mean	range	
TSP						
Mass	73.6	34.2	124.9	87.8	34.2	141.0
NO ₃ ⁻	12.1	5.2	19.5	16.7	5.2	28.8
NH ₄ ⁺	3.1	0.8	6.1	4.2	0.8	6.8
PM1.8						
Mass	22.5	10.6	30.2	26.7	10.6	41.7
NO ₃ ⁻	1.6	0.8	3.9	4.8	0.8	14.8
NH ₄ ⁺	1.6	0.7	2.5	2.5	0.7	4.8

Table 3.1: Summary of the mean and range of concentrations for the total mass, mass of nitrate and ammonium in TSP and PM1.8 as determined from filter based sampling ($\mu\text{g}/\text{m}^3$).

3.4 ATOFMS results

The hundreds of thousands of individual particles that were characterized by the 3 ATOFMS instruments can be sorted into categories that display the time series of particles having specific chemical attributes. Figure 3.2 shows the time series of carbon containing particles which is highest, as expected, in Riverside. This time series represents the total number of particles sampled by the ATOFMS instruments at a given site containing C^+ (mass/charge=12) in their individual particle mass spectra. The relatively high level of counts in Riverside reflects accumulation of the primary emissions from urban activities during air mass transport across the air basin, as shown in this figure.

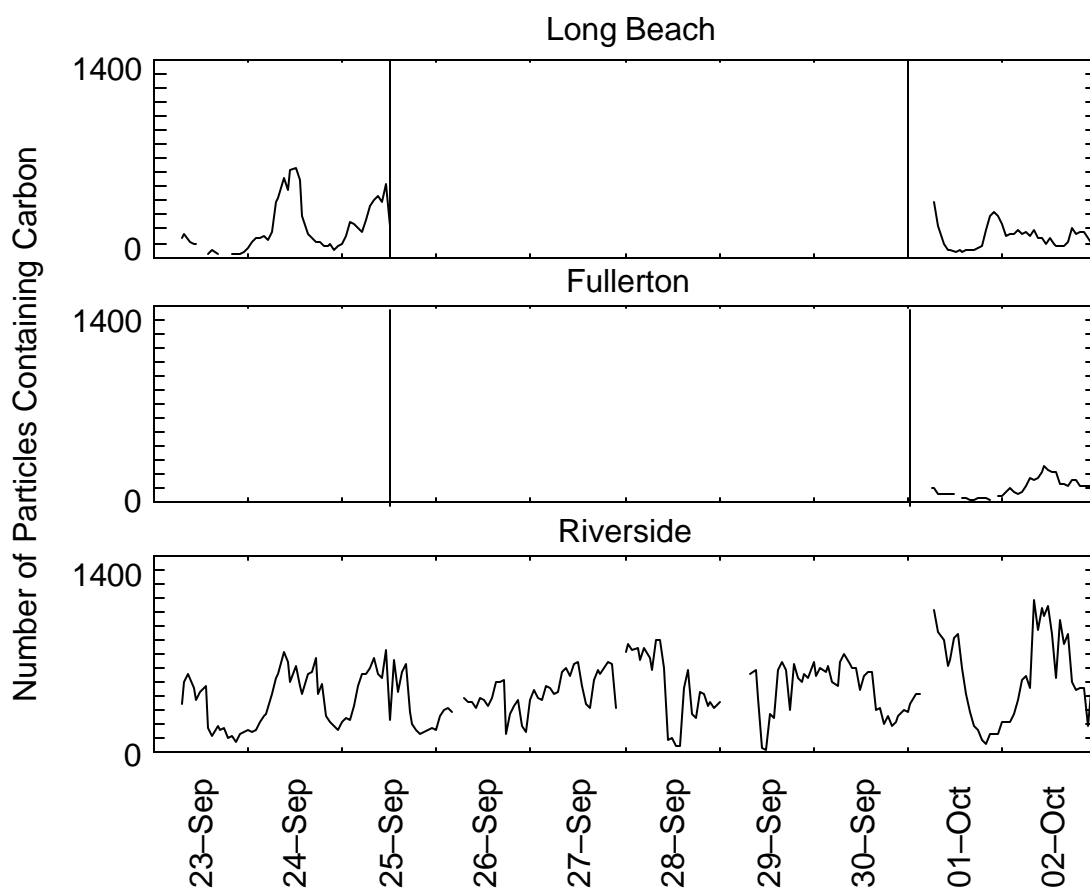


Figure 3.2: Total number of particles containing carbon (C^+) analyzed by the three ATOFMS instruments.

The time series of particle counts for particles containing ammonium and nitrate are shown in Figures 3.3 and 3.4. The time series appear to be identical, and indeed ATOFMS measurements directly show that ammonium and nitrate are generally found within the same individual particles in the fine mode ($< 1 \mu\text{m}$). The ability to definitively determine these associations is one of the major strengths of single particle mass spectrometry techniques. Close examination of the ammonium and nitrate containing particle counts shows the nitrate containing particles exceed the ammonium containing particles at Riverside on some occasions, for example on September 23-25 when sodium containing particle counts are elevated at Riverside, as shown in Figure 3.5. Sodium containing particles at these locations are typically indicative of sea salt derived particles. Not surprisingly the sea salt particle concentrations are highest at the coastal site at Long Beach.

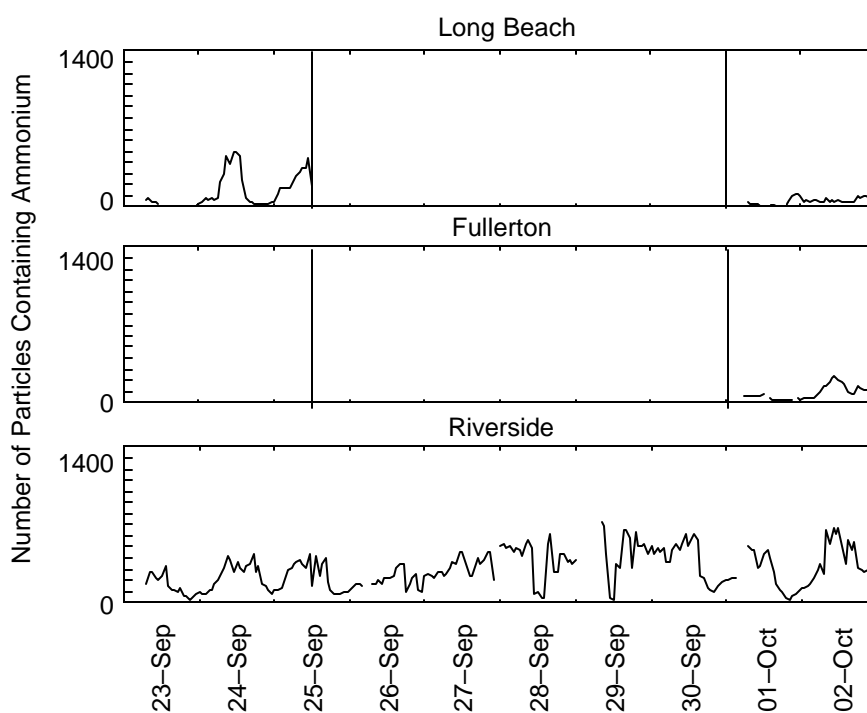


Figure 3.3: Total number (unscaled) of particles containing ammonium (NH_4^+) analyzed by the three ATOFMS instruments at each of the sampling sites.

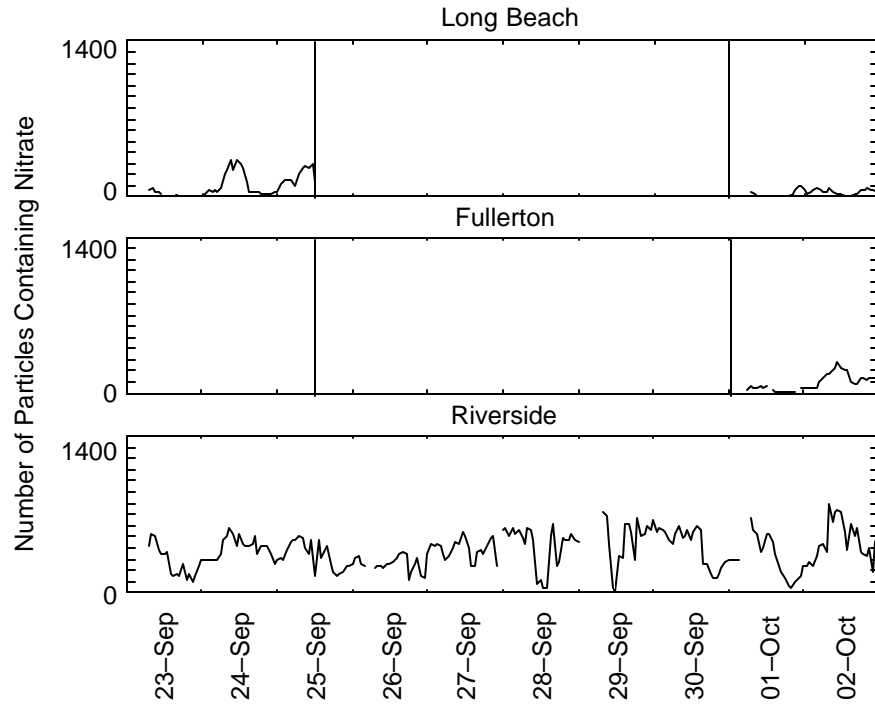


Figure 3.4: Total number (unscaled) of particles containing nitrate (NO^+) analyzed by the three ATOFMS instruments at each of the sampling sites.

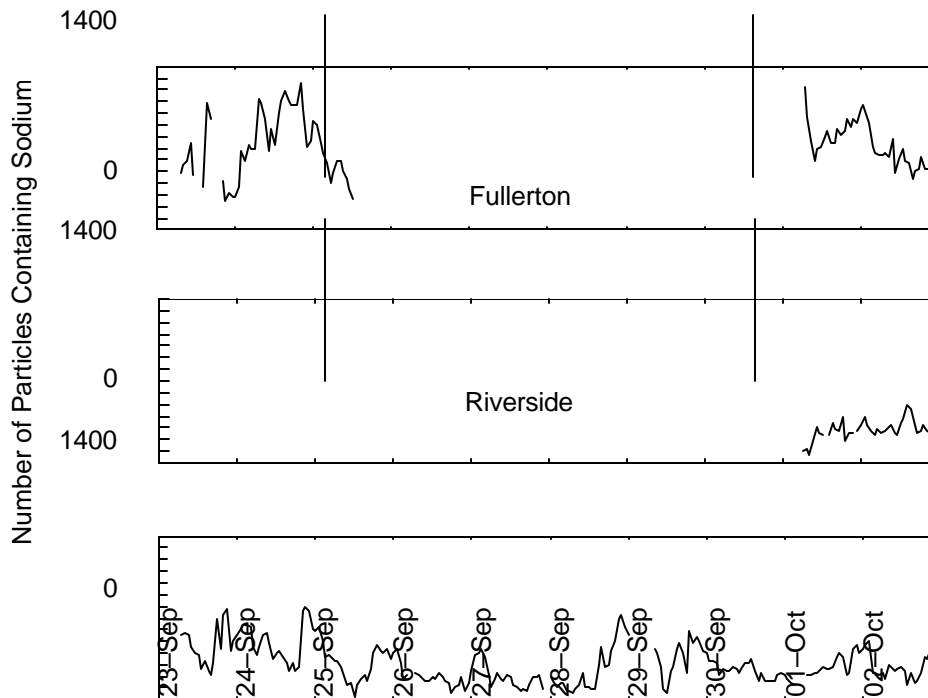


Figure 3.5: Total number of particles containing sodium (Na^+) analyzed by 3 ATOFMS instruments.

In fact, examination of single particle spectra show sodium nitrate particles to be present at Riverside during the times when there are higher nitrate counts than ammonium counts. Using ATOFMS data, it is quite evident that in general in the South Coast Air Basin there are two predominate forms of nitrate-containing particles, sodium nitrate and ammonium nitrate. Mass spectra of the two types of nitrate-containing particles are shown in Figure 3.6. Furthermore, in addition to differences in the composition of the two types of particles and thus sources, there are distinct differences in the size distributions of particles composed of sodium versus ammonium nitrate, as shown in Figure 3.7.

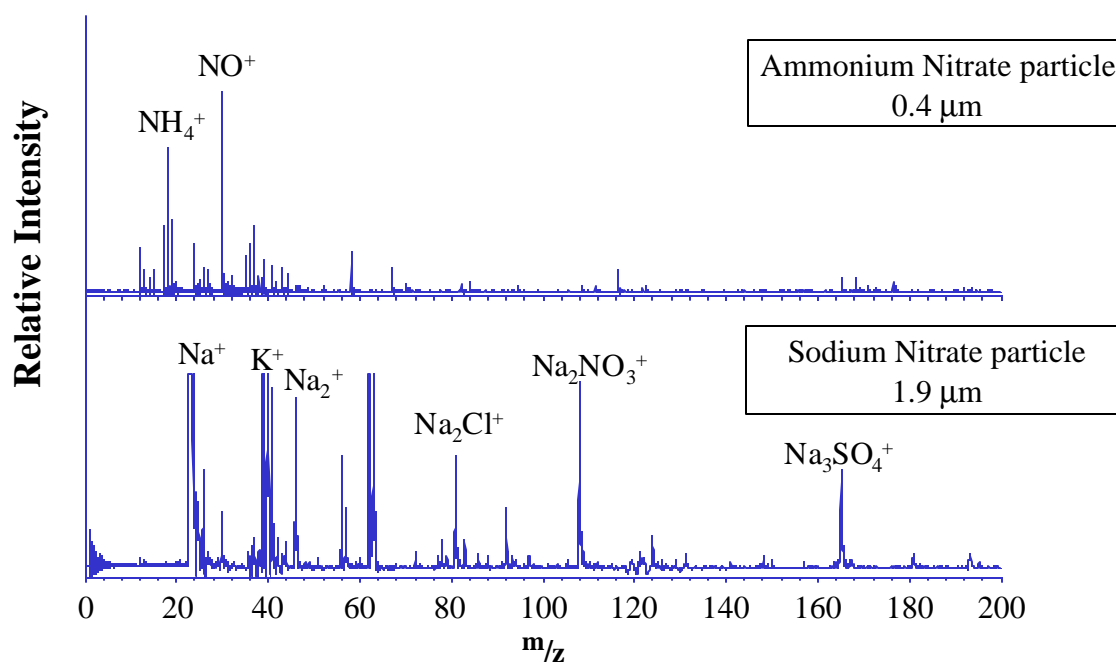


Figure 3.6: Mass spectra of two particles showing distinct types of nitrate, that coupled with ammonium and that coupled with sodium.

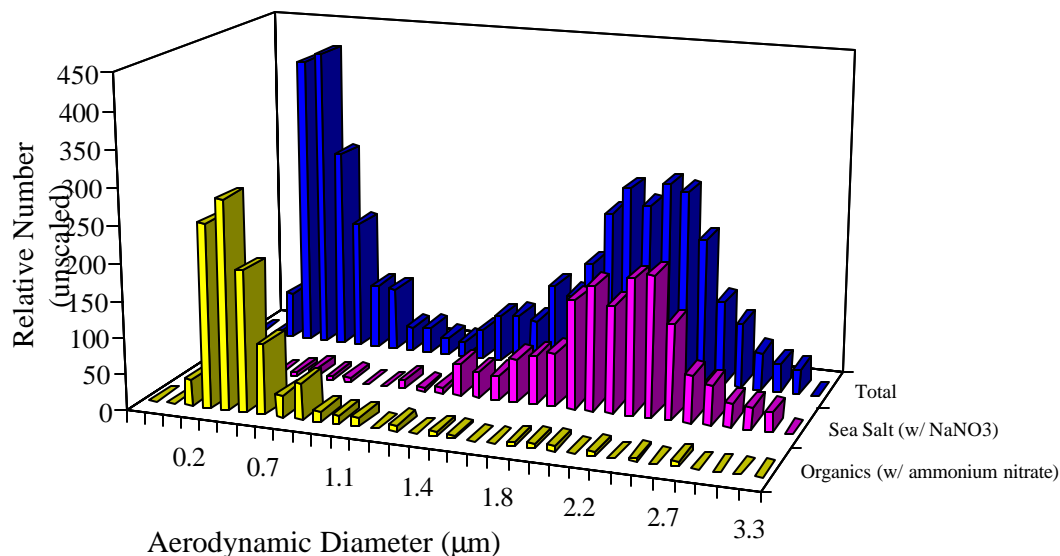


Figure 3.7: Difference in size distributions of sodium nitrate containing particles versus ammonium nitrate containing particles.

Examples of mass spectra of the characteristic particles used to create the time series shown in Figure 3.2-3.5 are shown in Figure 3.8-3.11. Figure 3.8 shows the mass spectrum of an ammonium nitrate containing particle of diameter $0.37 \mu\text{m}$. The key ions NH_4^+ and NO^+ are markers for ammonium and nitrate, respectively, and are accompanied by C^+ and C_3H^+ , indicating this particle was possibly composed of a secondary ammonium nitrate coating over a primary carbon particle core in a way that qualitatively matches many of the particles predicted by the air quality model of Kleeman et al. used for the sea salt reactions described in the next chapter (Kleeman, Cass et al. 1997). Figure 3.9 shows a $0.42 \mu\text{m}$ particle composed of hydrocarbons and little else. As is typical of many submicron particles, the carbon-hydrogen envelopes only extend out to C_3^+ or C_4^+ . Figure 3.10 displays the mass spectrum of an elemental carbon containing particle typified by fragments of integer numbers of carbon atoms with few or

no hydrogens attached. This particle also possessed a light coating of secondary ammonium nitrate. Finally, Figure 3.11 depicts the mass spectrum of a 1.77 μm sodium containing particle. This type of mass spectrum is typical of a sea salt particle in that it contains the common sea water cations Na^+ , K^+ , and Ca^+ along with smaller amounts of Na_3SO_4^+ , indicating sodium sulfate was present in the particle.

Our goal is to convert the data shown in this chapter into quantitative information on atmospheric aerosols. At this stage, determining the most appropriate ways to look at and utilize the types of information ATOFMS provides is a major focus of our research. The first procedures currently being utilized are discussed in the following chapters.

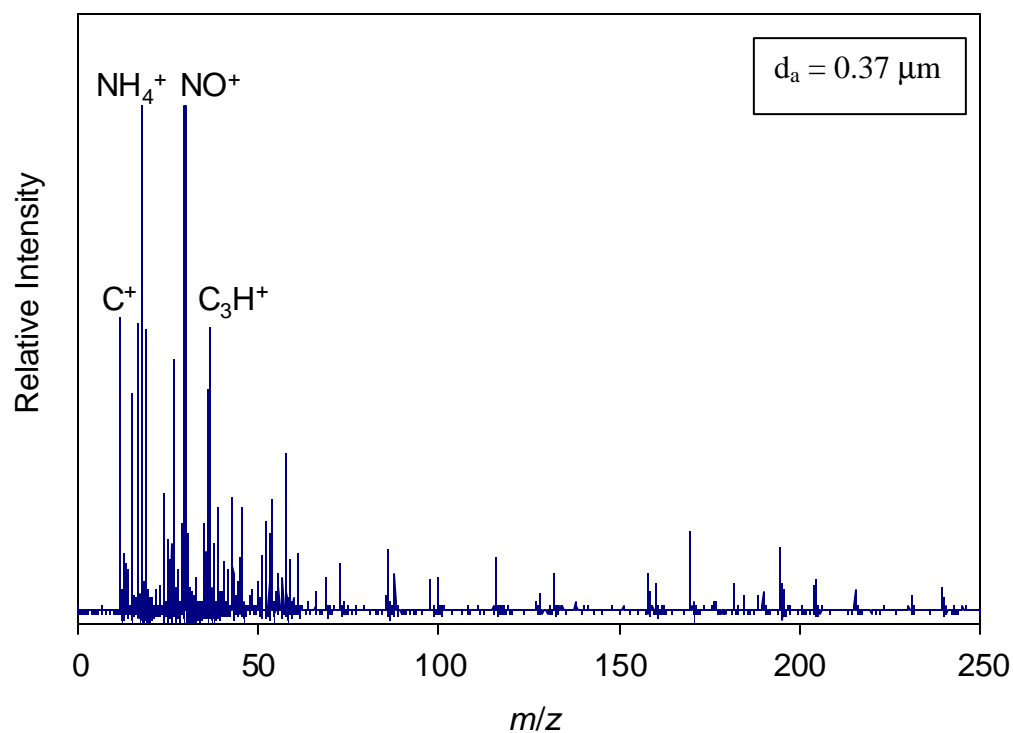


Figure 3.8: Mass spectrum of ammonium nitrate containing particle with peaks at mass-to-charge 18 (NH_4^+) and 30 (NO^+).

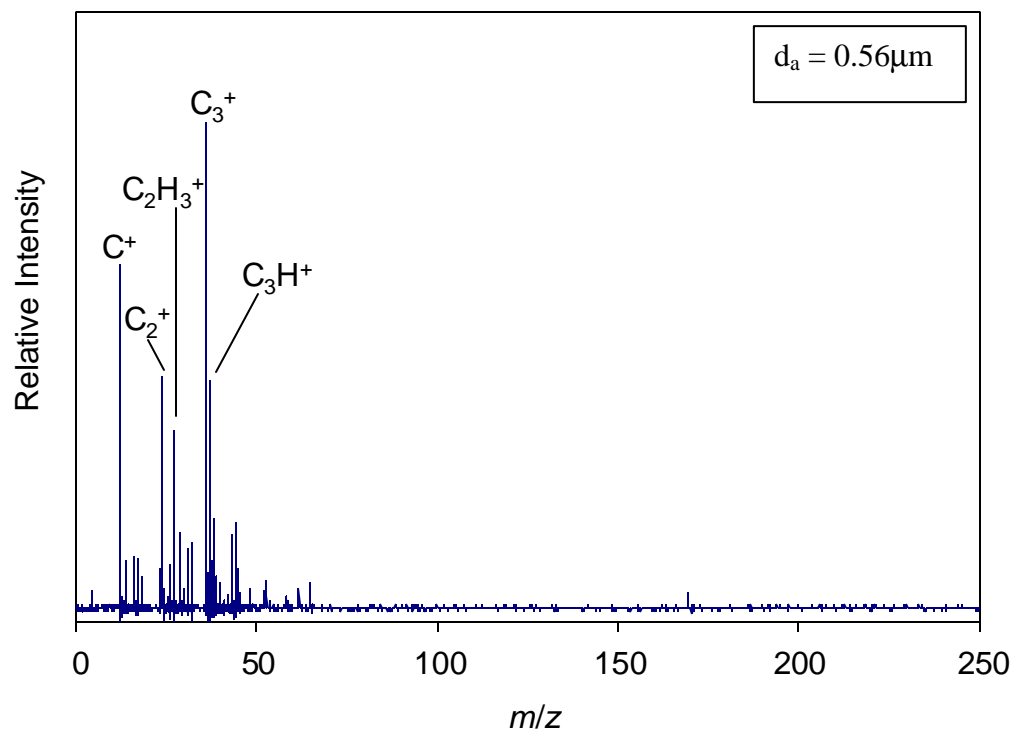


Figure 3.9: Mass spectrum of particle with organic components.

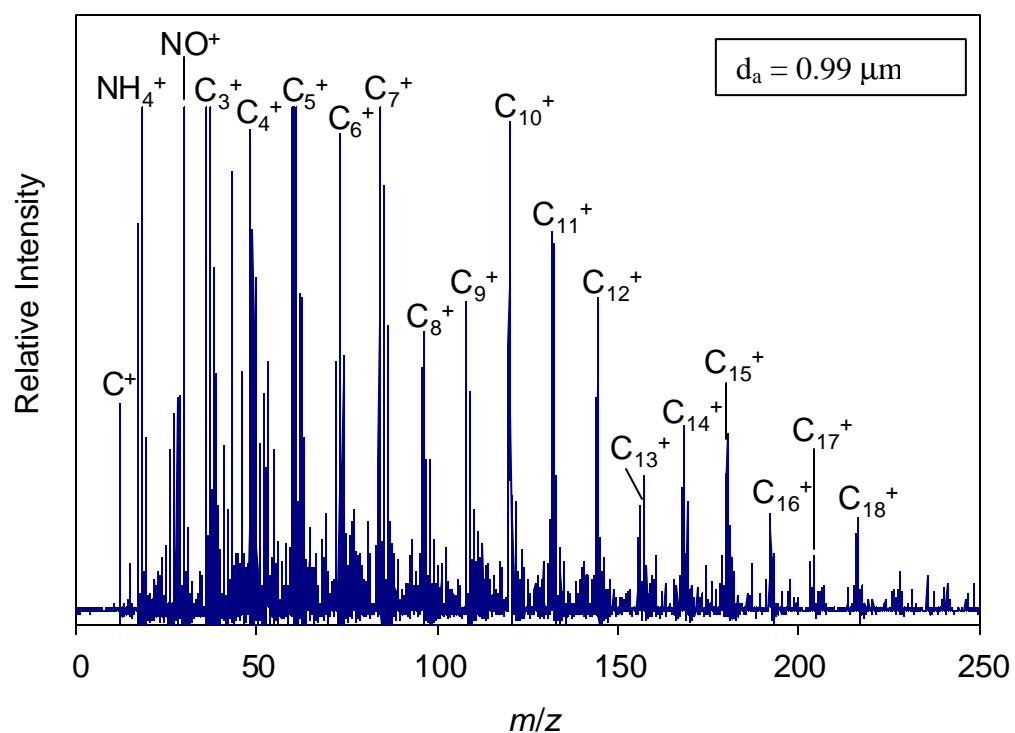


Figure 3.10: Mass spectrum of elemental carbon containing particle.

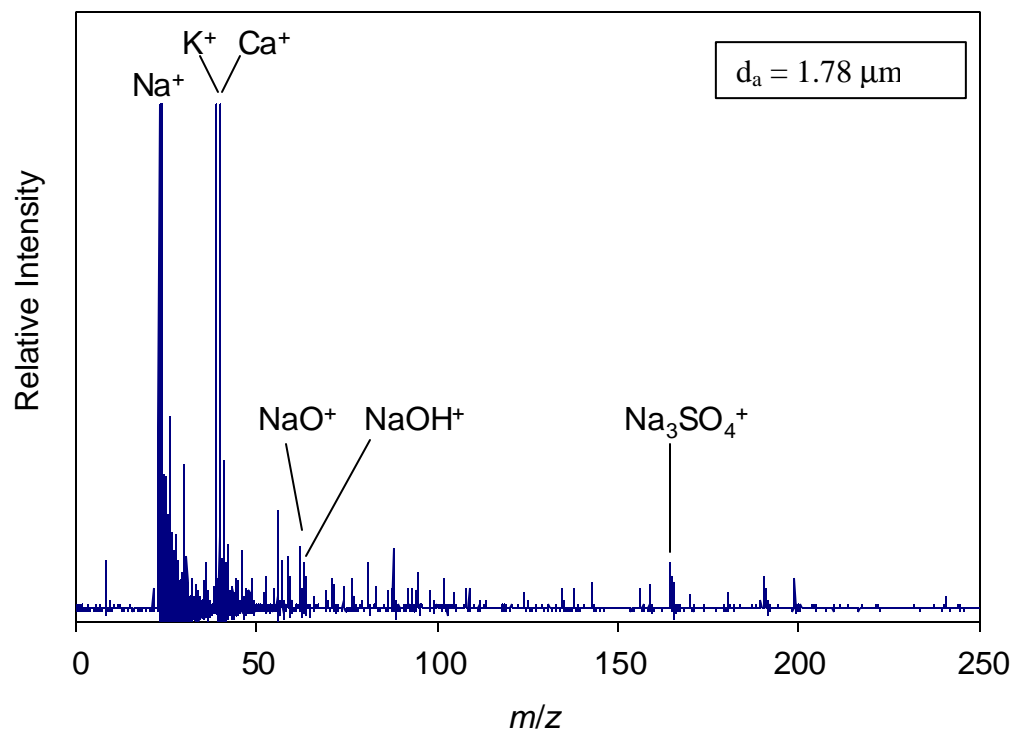


Figure 3.11: Mass spectrum of sodium containing particle (sea salt).

Chapter 4

Sea Salt Chemistry in Long Beach

4.1 Background on sea salt chemistry

The role of biogenic and anthropogenic aerosols in the global atmospheric cycle and their effects on human health are intriguing and topical issues. Anthropogenic aerosols are believed to have a net negative effect on the earth's radiation budget. This has been used to explain why the magnitude of the observed global temperature increase due to greenhouse gases has been moderated as compared to the predictions of climate models. This, however, is still a topic of much debate. In addition to their potential global impact, aerosols have been linked to increased respiratory illness, morbidity, and premature mortality in humans. Given their wide ranging importance spanning from global to personal levels, it is important to develop and use new methods and models to try and gain a detailed understanding of particle formation, evolution, and fate in the atmosphere. This will allow development and access of rational regulatory measures which can be used to address the impact of both biogenic and anthropogenic aerosols on the global and local scales.

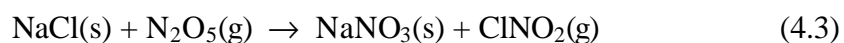
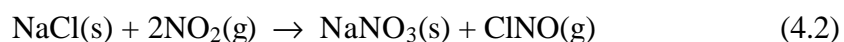
In order to fully understand and, hence, predict the spatiotemporal variations in the chemical and physical properties of ambient tropospheric aerosols, one must first know the temporally and spatially resolved emission inventories from all relevant gas and particle sources. In addition, air parcel trajectories, meteorology, gas-phase chemical reactions, diffusion of gases to and from particles, heterogeneous and multiphase chemistry, and dry deposition processes must all be considered in order to track the gas-phase and particle-phase composition fluxes over time and space.

This kind of comprehensive treatment of aerosols is achieved through the use of mechanistic air quality models which track primary emissions of particles and gases in the atmosphere as these pollutants undergo dilution, reaction, and deposition. Recently, a source-oriented external mixture model has been developed which tracks discrete particles having initial sizes and chemical compositions determined by the source from which they were emitted, as they are advected across an airshed (Kleeman, Cass et al. 1997). The critical difference between this and previous model formulations is that in a source-oriented external mixture, particles of the same size can evolve to display different chemical compositions that depend on the chemical and hygroscopic properties of the primary seed particles initially emitted from different sources. In contrast, previous models treat the airborne particles as an internal mixture in which all particles of the same size are assumed to have the same chemical composition.

Despite the existence of these evolving external mixture models which can effectively predict temporal variations in the size and composition of individual particles, assessing their efficacy has generally relied on comparing the model predictions to bulk chemical analysis of particles collected on filters and gas-phase measurements. Unfortunately, the poor experimental time resolution used to sample particulate matter coupled with bulk chemical analysis precludes comparing particle information from model and experiment at a level beyond the temporally and chemically homogenized mixtures that are collected on filters. However, the recent invention of portable aerosol time-of-flight mass spectrometers which are capable of measuring both the size and chemical composition of individual particles in real-time provides a tool to evaluate these more detailed models at the individual particle level.

Some of the most extensively studied heterogeneous reactions involve sea salt reactions such as those shown below in 4.1-4.4 (Finlayson-Pitts and Pitts Jr. 1986; Pszenny and al. 1993;

Vogt, Elliott et al. 1996; Langer, Pemberton et al. 1997; Ravishankara 1997). One commonality to all of these reactions is the depletion of chloride and accumulation of nitrate in the reacting particles.



Given the relatively high concentrations of HNO_3 , Reaction 4.1 most likely accounts for a substantial portion of the observed conversion of chloride to nitrate in sea salt in the South Coast Air Basin. This is the only heterogeneous sea salt process that is currently incorporated in the model. This is an ideal reaction to monitor in a study of this type in that Reaction 4.1 is one of the most extensively studied heterogeneous chemical reactions in the laboratory using a wide variety of techniques (Bruynseels and Van Grieken 1985; Leu, Timonen et al. 1995; Beichert and Finlayson-Pitts 1996). These laboratory studies have provided significant insight into the mechanisms, kinetics, and thermodynamics of the reactions, however none of these experiments can be certain of exactly duplicating atmospheric conditions. To date, all of these studies arrive with different conclusions because of the difficulty involved in accurately simulating atmospheric conditions and sea salt concentrations.

This chapter focuses on the marine chemistry experimentally observed and modeled in Long Beach, California from midnight on September 23 until midnight on September 25 PST. This provides the first opportunity to qualitatively compare the real-time information from the ATOFMS instruments with the predictions of a source-oriented external mixture model at the

single particle level. The primary goals of this study were to test the performance of the newly constructed ATOFMS instruments, as well as to demonstrate the feasibility of using them in the field. The results described in this chapter and the following ones demonstrate the first study accomplished these goals.

4.2 Experimental: ATOFMS

Details of the transportable ATOFMS instrument have been presented in Chapter 2. Briefly, particles are sampled directly from the ambient atmosphere into the ATOFMS through a convergent nozzle, and then pass through three stages of differential pumping. During this process, particles are accelerated to a terminal velocity proportional to their aerodynamic diameter ($d_a = \sqrt{\rho \cdot d_p}$). This velocity is measured by detecting light scattered from the particles as they cross two orthogonal continuous wave laser beams, located a known distance apart. The time between the two pulses of scattered light is measured by a timing/logic circuit, and is used to trigger a pulsed Nd:YAG laser (266 nm) to fire when the particle reaches the center of the source of a dual co-linear-reflectron time-of-flight mass spectrometer. Thus, both the size and composition are obtained on the individual particle level for polydisperse aerosol samples.

In the first field study, only positive ion mass spectra were acquired. The dual ion capabilities of the transportable instruments were not functioning until after this study was complete.

4.3 Results: ATOFMS

A transportable ATOFMS instrument, located in Long Beach, California (~2 miles east of the Pacific Ocean), acquired the size and positive ion mass spectra of roughly 1000 particles per hour and was operated nearly continuously for the two day period of interest. As expected, given the site's proximity to the ocean, the dominate particle type observed was sea salt, which is

readily identified by the presence of Na^+ ($m/z = 23$), K^+ ($m/z = 39$), $\text{Na}_2^{35}\text{Cl}^+$ ($m/z = 81$), and $\text{Na}_2^{37}\text{Cl}^+$ ($m/z = 83$) ion peaks in the positive ion mass spectra. In order to confirm that the marine particles in this study are in fact sea-salt, the ratio of the relative intensities of Na^+ and K^+ can be compared to that in sea-water using an empirical relative sensitivity factor (RSF) (section 5.6). The measured RSF for K^+/Na^+ is 5.1 (Gross, Gaelli et al. 1998). While sea salt particles are identified based strictly on composition, they also have a characteristic aerodynamic diameter greater than $1.0 \mu\text{m}$ which helps corroborate their source. In addition, a continuously varying percentage (10 - 50 %) of fine ($<1 \mu\text{m}$) organic particles was the other significant particle type observed at this location. These organic particles are characterized by an aerodynamic diameter less than $1.0 \mu\text{m}$ and mass peaks corresponding to hydrocarbon envelopes containing from one to five carbons (similar to the mass spectra shown in Figures 3.8-3.10).

The temporal variations of chloride and nitrate in sea salt particles are investigated by monitoring the relative intensity of their mass spectral markers with time. Markers for these species in the positive ion mass spectra are Na_2Cl^+ (m/z 81 and 83) and Na_2NO_3^+ (m/z 108), respectively (Figure 4.1).

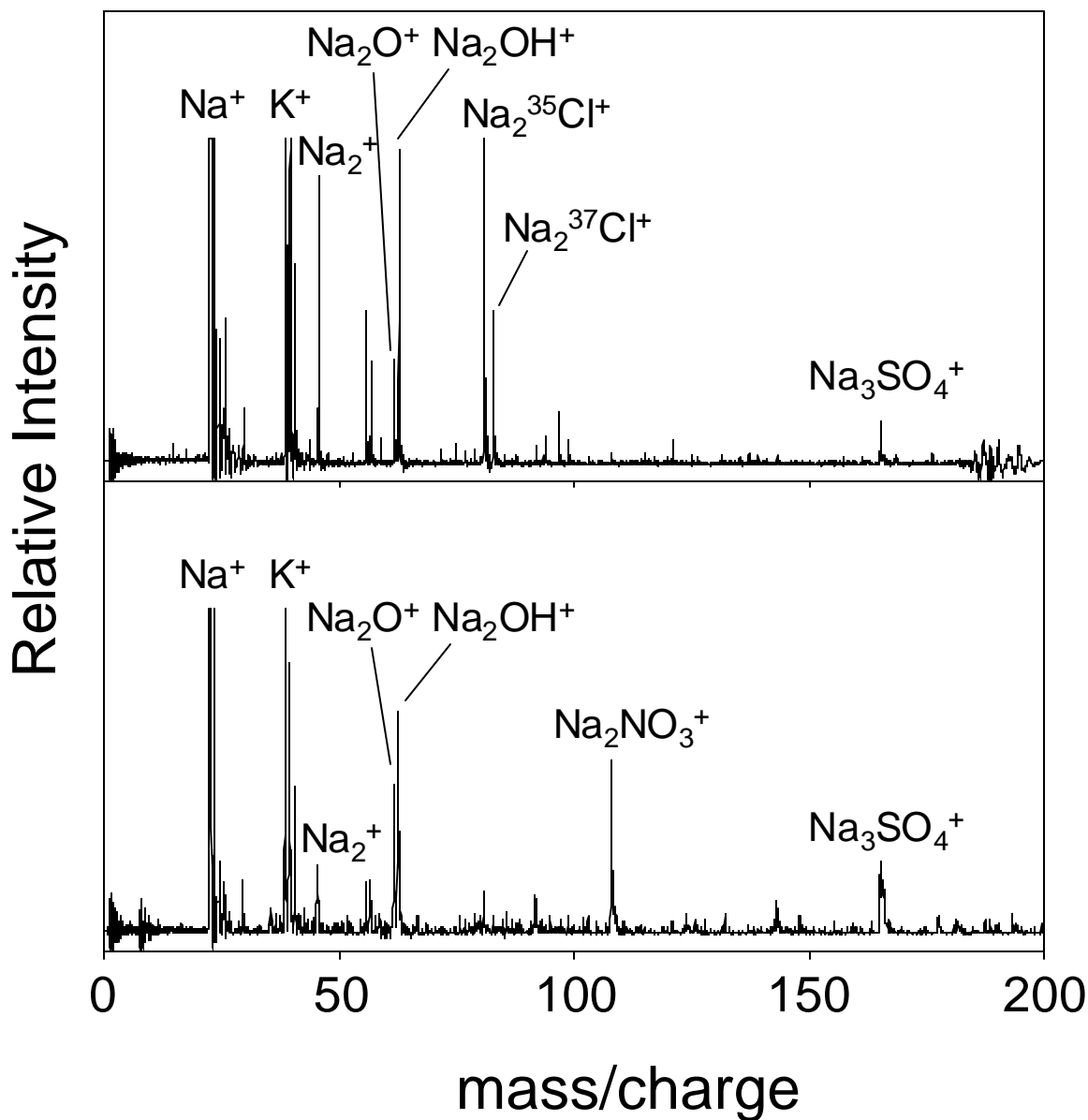


Figure 4.1: Two positive ion mass spectra of sea salt particles. The top figure shows the spectrum of an unreacted particle and the bottom shows a reacted particle.

Using a single particle perspective, an informative way to determine the extent of reaction of the sea salt particles at any given time is to plot the relative intensity of the product ion peaks (sodium nitrate) against the relative intensity of the reactant ion peaks (sodium chloride), as shown in Figure 4.2.

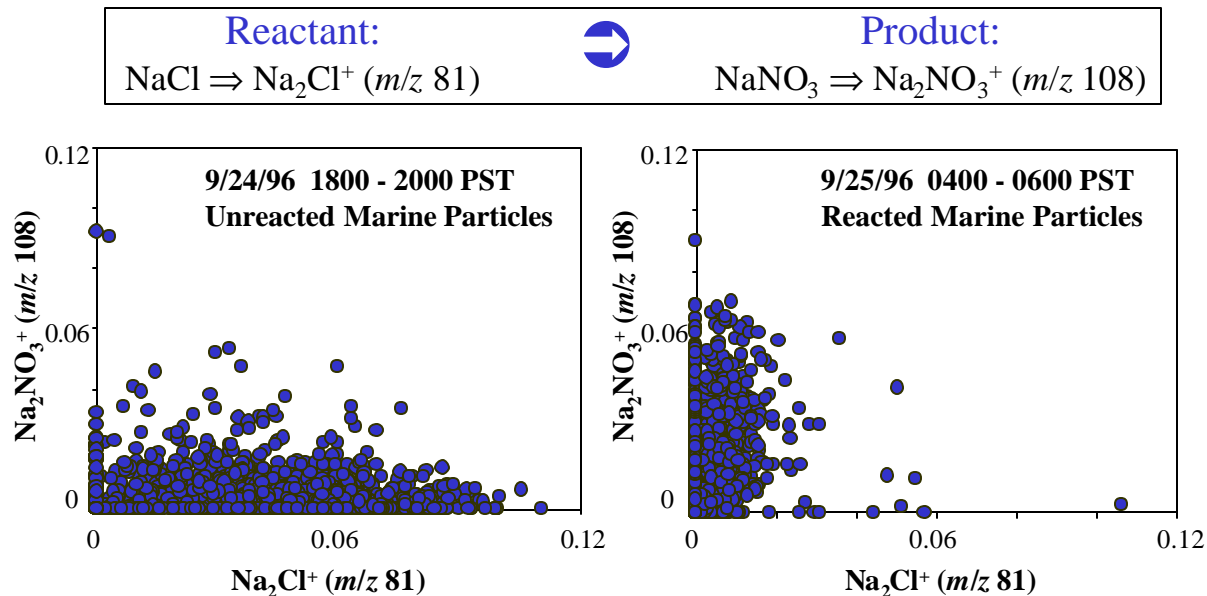


Figure 4.2: Tracking conversion of ion abundance of reactant ions (Na₂Cl⁺) to product ions (Na₂NO₃⁺) in individual sea salt particles.

In Figure 4.2, one can see that when the sea salt particles are unreacted, most of the data points lie along the x-axis, indicating relatively small amounts of sodium nitrate (product) and relatively high amounts of sodium chloride (reactant). In contrast, as shown in the graph on the right, as the particles react to form sodium nitrate there is a shift of the data points to the y-axis, indicating higher amounts of reacted sea salt.

One can view this same plot as it evolves over time moving between these two extremes by collecting and averaging the relative intensity of the ion peaks representing Na₂Cl⁺ and Na₂NO₃⁺ in all spectra containing peaks corresponding to Na⁺, K⁺, Na₂Cl⁺ and/or Na₂NO₃⁺ in one-hour time bins. This time resolution is chosen to match that of the model. Diurnal trends are immediately evident when the average relative intensity of these peaks are plotted versus time (Figure 4.3). Each data point from the ATOFMS represents the average of the relative intensities of the marker peak in all sea-salt particle mass spectra acquired during the time of interest. The mass concentrations for nitrate measured in Long Beach are reported in Table 3.1.

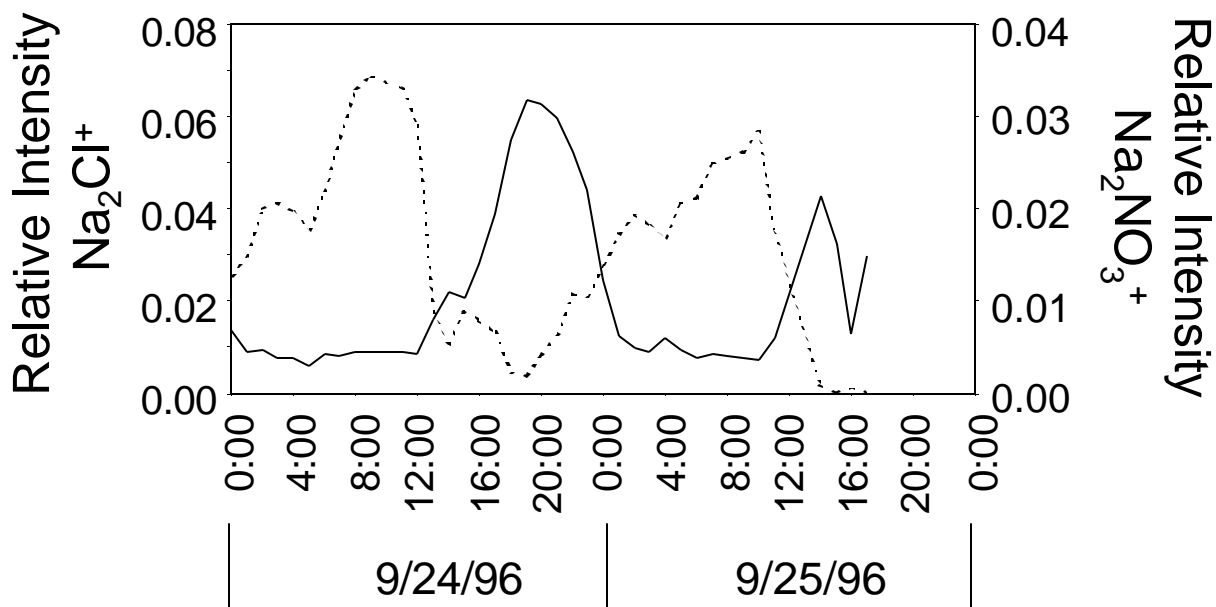


Figure 4.3: Plot showing amount of sodium nitrate (product) versus sodium chloride (reactant) in single sea salt particles sampled by ATOFMS over a two day period in Long Beach, CA.

4.4 Model

In an effort to model the ATOFMS measurements, a source-oriented external mixture trajectory model was used to predict the levels of nitrate and chloride in sea salt particles during the observation times (Kleeman, Cass et al. 1997). Meteorological data was obtained from field observations, while emissions inventories were taken from the August 28, 1987 SCAQS episode (Eldering and Cass 1996). Forty eight trajectories ending at the Long Beach sampling site on each hour of the days September 24 – September 25, 1996 were calculated (Figures 4.5 and 4.6).

To compare the model results to the ATOFMS data, the marine particles in the model with aerodynamic diameters less than $2.5 \mu\text{m}$ from each trajectory calculation were isolated from those of anthropogenic origin. The upper limit of $2.5 \mu\text{m}$ particle diameter was chosen as the best match between size bins used to track particles in the model calculation and the inherent transmission efficiency of the ATOFMS inlet nozzle, which transmits particles below $3 \mu\text{m}$ with

high efficiency. Within each hourly trajectory the relative molar content of chloride and nitrate was then calculated for each particle and averaged.

Model results show a strong diurnal variation, with chloride and nitrate anti-correlated (Figure 4.4). The chloride signal is high at night, while nitrate signal is high during the day, demonstrating remarkable qualitative agreement with the trends observed by the ATOFMS.

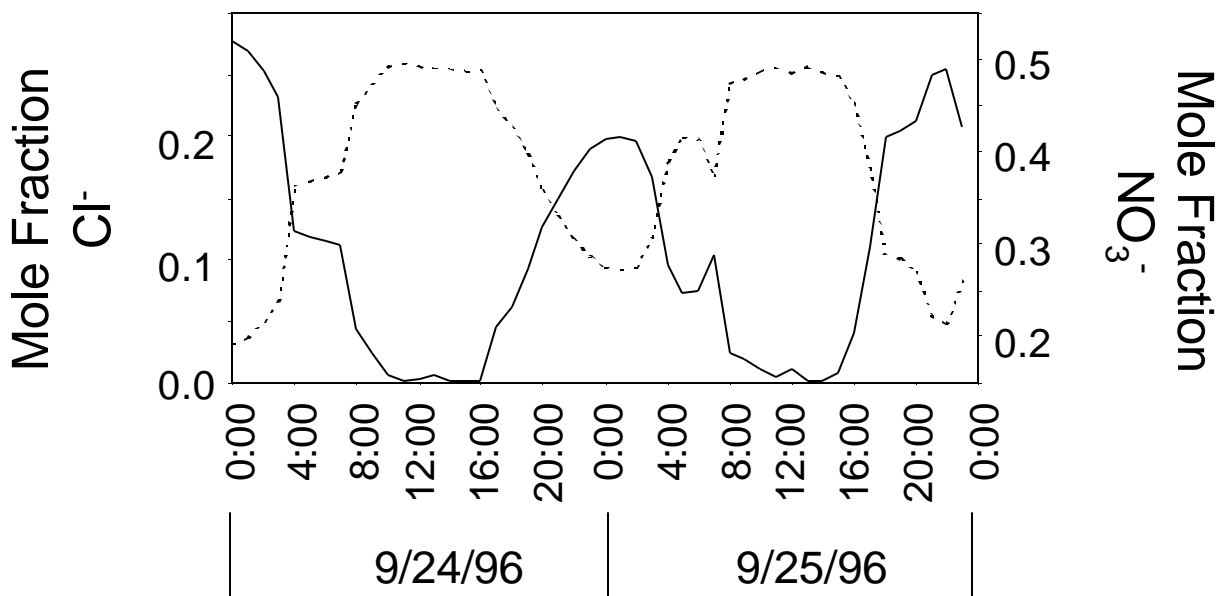


Figure 4.4: Results of model predicting concentration of chloride and nitrate in sea salt particles during time of sampling.

Using the history of each air trajectory, one can interpret the ATOFMS and model results, accounting for the observed diurnal cycle. First, sea salt particles (composed primarily of NaCl) are generated by the action of breaking waves at the coastline. As these particles are advected inland, they encounter a variety of anthropogenic and biogenic gas-phase emissions which initiates heterogeneous/multiphase chemistry. Gas-phase HCl and HNO₃ concentrations in the Los Angeles basin are typically at levels which drive the thermodynamically favorable displacement of chloride by nitrate in sea salt particles by Reaction 4.1. The extent to which this reaction occurs is affected by many factors including: gas phase concentrations, particle phase

concentrations, temperature, relative humidity, and reaction time.

The relative concentration of chloride in the marine particles peaks during the late afternoon until the early morning hours of each day because the air parcels arriving in Long Beach were swiftly transported from the coastline, providing little time for the reaction to occur. This is shown in Figure 4.5, the 48 hour trajectory of the air mass obtained from meteorological data. Working back from the sampling point in Long Beach, each circle represents where the air mass was the hour before.

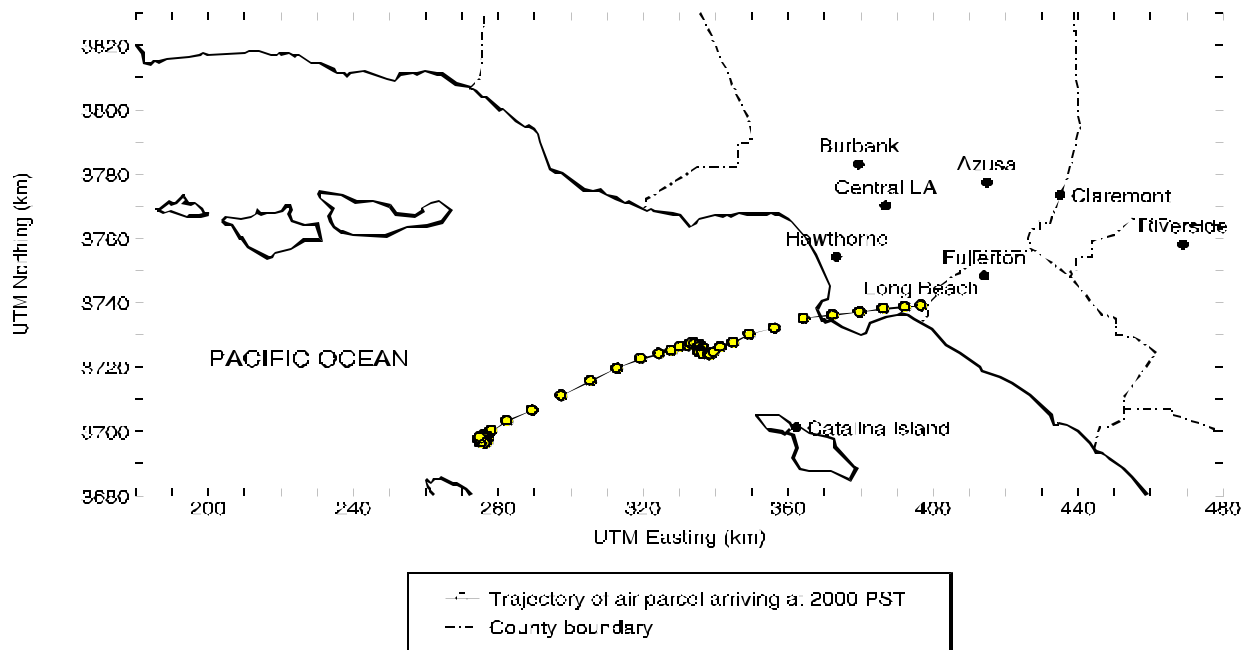


Figure 4.5: Air trajectory of air mass showing transport from sea with no stagnation over land before sampling point, producing relatively unreacted sea salt in air mass.

In contrast, during the late morning to early afternoon of each day, when nitrate in the sea salt particles dominates, the air parcels that arrive at the sampling site have stagnated over land during the night; allowing the reaction to proceed further towards completion (Figure 15).

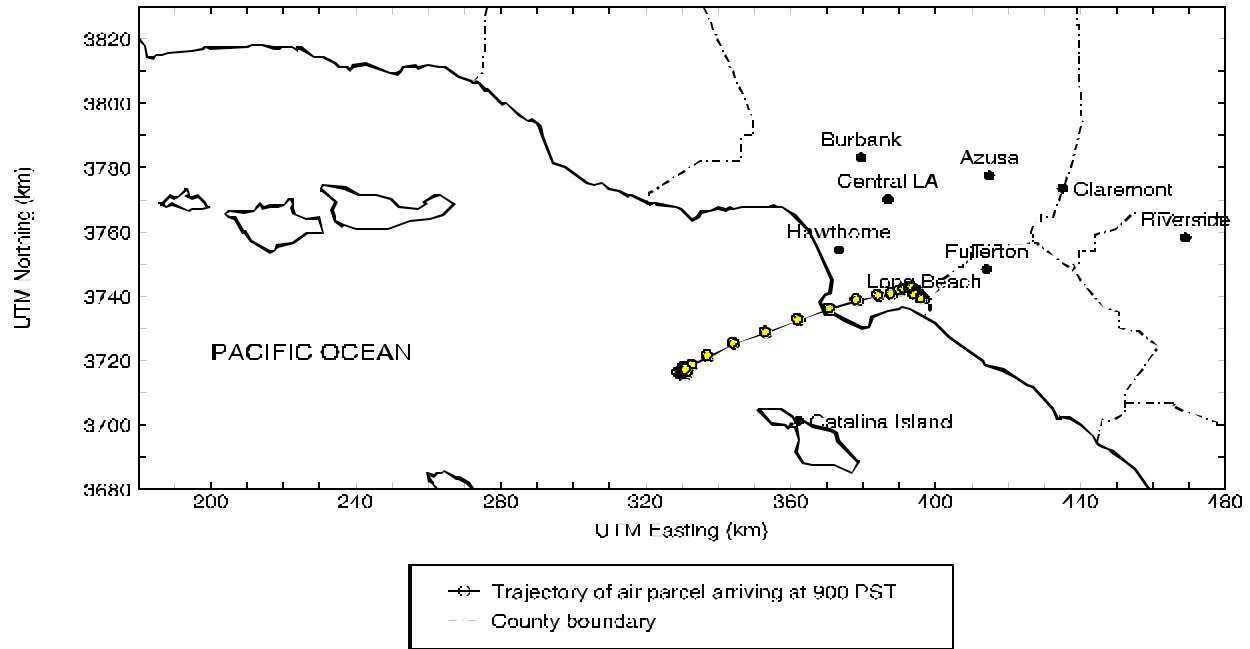


Figure 4.6: Air trajectory of air mass showing transport from sea with some stagnation over land before sampling point, producing relatively more reacted sea salt in air mass.

4.5 Conclusion

A key factor in determining the chloride/nitrate oscillations observed at Long Beach on September 24-25, 1996 is the amount of time the displacement reaction has to occur. At the time of the experiment, meteorological data show that the same air mass stagnated over the Long Beach sampling site for 11 hours from approximately 24:00 hours PST on September 24 to 11:00 hours PST on September 25, 1996. The effect of reaction time on particle phase concentrations is clearly illustrated by plotting the amount of time each air parcel spends over land against the sodium nitrate (product) concentrations observed in individual sea salt particles using ATOFMS (Figure 4.7).

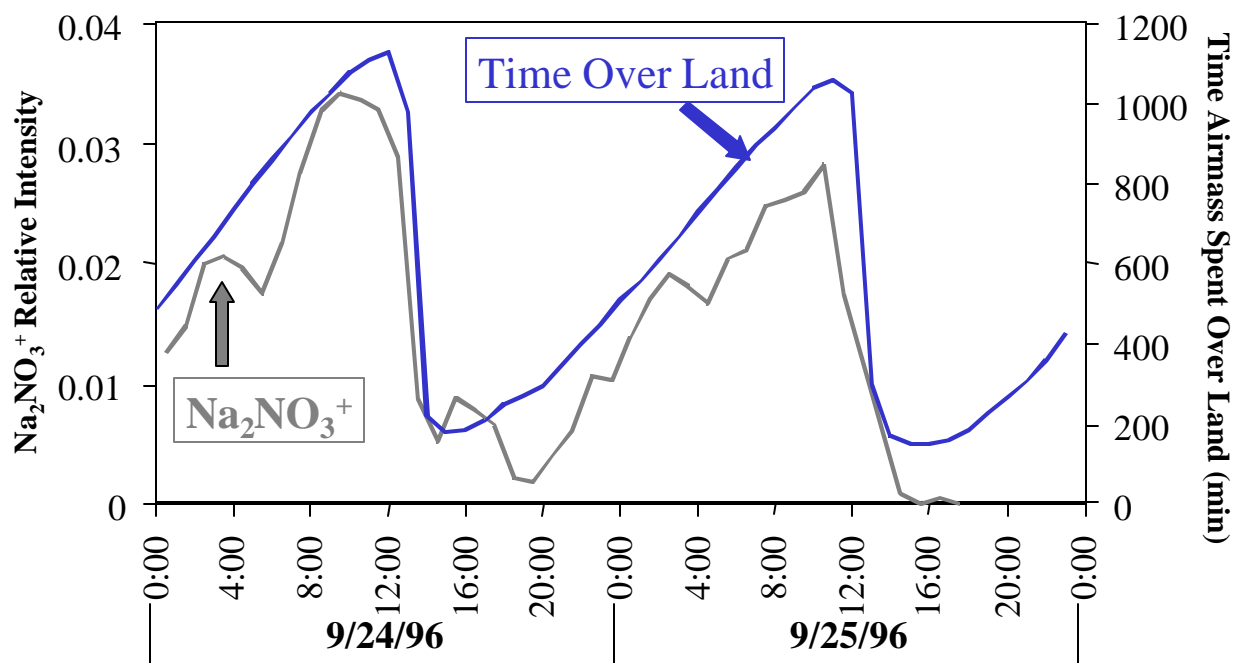


Figure 4.7: Plot showing the amount of product (sodium nitrate) in single particles is directly correlated with amount of time particles spent over land or total reaction time.

4.6 Summary of sea salt study

The unique measurement capabilities of the ATOFMS instrument used for these experiments, real-time results, and most importantly *transportability*, make such a study possible. In addition, the acquisition of such data makes it possible for the first time to compare the output of real-time single-particle based models of tropospheric aerosols, such as the source-oriented external mixture trajectory model, to ambient processes at the single-particle level. The data presented here represent the first demonstration of heterogeneous reactions occurring on individual ambient aerosol particles that have been measured in real-time. In addition, the results of this study demonstrate the potential knowledge that can be gained by making comparisons between real-time single-particle based models and measurements, an effort that has provided good qualitative agreement. As one would expect given the complexity of the measurements and model, the agreement is not perfect but the general trends are consistent. For a first effort, this

study provides promise that now measurements can be made at the single particle level which can be used to provide feedback to the model. In the process, the major factors that affect the observed aerosol chemistry will be determined, thereby developing a better understanding of aerosol processes in the atmosphere.

Chapter 5

Quantification

5.1 Overview of Field Experiment

As described in Chapter 3, the first field study using the transportable ATOFMS instruments was conducted in late September and early October of 1996. Results on the heterogeneous chemistry observed in this study are reported in Chapter 4 of this report. As described, three sites were strategically chosen in order to capture the chemistry occurring on particles in an air mass as it was advected inland from the ocean. These sites were located in Long Beach, Fullerton, and Riverside, CA. The two newly constructed transportable ATOFMS instruments sampled at Long Beach and Fullerton, while a lab-based ATOFMS sampled in Riverside. Also at each of the sites were a host of other analysis equipment including electrical aerosol analyzers and optical particle counters for particle size distribution measurements and inertial impactors and bulk filter samplers for measuring the size resolved chemical content of the particles.

5.2 Goals of Study

The ATOFMS instruments acquire data in the form of single particle mass spectra and number distributions as a function of aerodynamic diameter. These number distributions represent raw particle counts. ATOFMS counting efficiencies are biased towards larger (i.e. supermicron) sizes due to factors including transmission, scattering, and detection efficiencies of single particles (Allen, J. et al. 1999). In order to obtain a statistical representation of the composition of all particles over the size range between 0.1 and 2.5 μm , this bias is required.

Otherwise, one would just observe only small particles due to their much larger number concentrations. However, in order to obtain size distributions that are representative of those in the atmosphere, one must be able to establish conversion factors that allow one to convert from raw ATOFMS number counts to scaled mass distributions. There are two ways to accomplish determining the appropriate conversion factors. The first involves directly determining transmission and detection efficiencies of the ATOFMS instruments by calibrating the instruments using known concentrations of particles of differing sizes. This research is currently being conducted in our lab. The second way, and the one performed as part of this study, involves sampling particles alongside MOUDI impactors which obtain mass distributions as a function of size. Then by comparing ATOFMS number distributions of particles as a function of size with the MOUDI mass loadings in different size bins, the appropriate ATOFMS scaling factors can be derived. A goal of these studies is to determine how much the scaling factors change over the course of the experiment.

5.3 Results

ATOFMS obtains precise size information but in order to compare it with the mass concentrations from the MOUDI impactors, the number counts of particles must be grouped into size bins identical to those of the impactor. Grouping the particles into size bins results in a loss of ATOFMS information; however, it represents a reasonable starting place for making a comparison between ATOFMS and MOUDI data to determine if correlations exist in the data under the conditions of the field study, sampling “real” atmospheric particles. In Section 5.3, results from an alternate approach are presented where size grouping is not required.

ATOFMS calibration can be accomplished by performing side-by-side sampling between the ATOFMS instruments and MOUDI impactors at the same times and locations. Scaling

factors may be calculated by comparing the total number of particles detected by the ATOFMS instrument with the mass sampled over the same time by a MOUDI in each of the impactor size bins. Total ATOFMS particle counts are converted to mass loadings ($\mu\text{g}/\text{m}^3$) for each of the MOUDI size bins assuming a particle density of $1.7 \text{ g}/\text{cm}^3$. Scaling factors may be calculated using Equation 5.1. Figure 5.1 shows scaling factors that represent averages of multiple 4-hour side-by-side sampling periods in Long Beach, Fullerton, and Riverside. As shown in this figure, the factors for the 2 transportable ATOFMS instruments are similar. However, the factors needed for lab-based instrument in Riverside are substantially lower than those for the transportable instruments. This can be attributed to the lower powers on the scattering lasers as well as differences in the inlet geometries. This was due to the fact that the transportable instruments had just been assembled prior to this study and thus allowing very little time for optimization of the instruments. It should be noted that subsequent to this study, the transportable instruments were optimized and smaller scaling factors are now necessary for converting the data. The scaling factors shown in Figure 5.1 remained relatively constant over the duration of the field study indicating ATOFMS number counts can be used to reliably indicate the actual atmospheric particulate mass loading over the entire field study (i.e. not just during intensive sampling periods).

$$\text{Scaling Factor} = \frac{\text{Impactor mass loading } (\mu\text{g}/\text{m}^3)}{\text{Calculated ATOFMS Particle Mass } (\mu\text{g})} \quad (5.1)$$

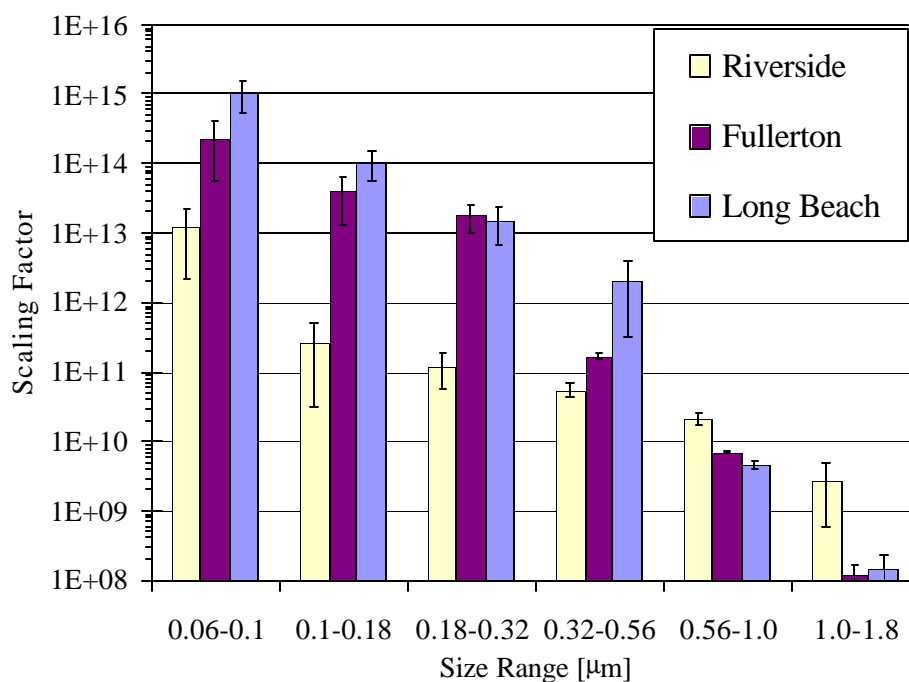


Figure 5.1: Scaling factors used to convert ATOFMS number distributions to mass distributions as determined by comparison with simultaneously acquired MOUDI data.

Using the scaling factors in Figure 5.1, mass distributions can be obtained from the raw ATOFMS number counts. Figure 5.2 shows a representative comparison of the calculated mass loadings for the ATOFMS and MOUDI impactors sampled during an intensive sampling event in Long Beach, CA. As described, the scaling factors allow for conversion of raw particle counts obtained by the ATOFMS instruments to mass distributions. One of the goals of the study is to be able to obtain mass loadings for specific chemical species including nitrate, sulfate, ammonium, metals, organic and elemental carbon. The ATOFMS instruments are expected to possess different sensitivities for each of these different species. Results from studies aimed at determining these sensitivities will be reported in future publications. Details of lab studies aimed at determining the relative response factors for various species are provided at the end of this chapter in Section 5.6.

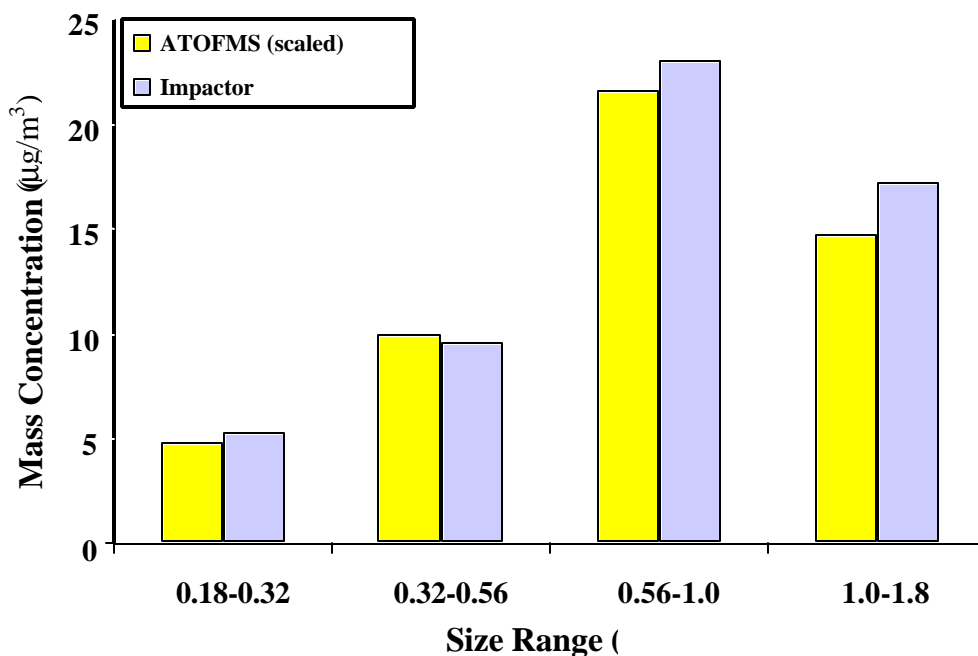


Figure 5.2: Comparison of mass concentration obtained for ATOFMS versus MOUDI acquired over a 4 hour period on September 25, 1996.

It is extremely difficult to accurately simulate atmospheric aerosols in lab studies aimed at developing accurate relative sensitivity factors. Another approach involves comparing ATOFMS particle counts for a particular chemical species versus MOUDI impactor mass loadings for the same compound in atmospheric samples. In order to do this, one must establish appropriate markers in the single particle mass spectra which are indicative of the species of interest. In the case of ammonium and nitrate, positive ion peaks at mass/charge 18 and 30 (NH_4^+ and NO^+) have been determined appropriate in lab studies using particles of known composition.

In the field study during the intensive sampling periods, all of the particles with an ion peak in their mass spectra at mass/charge 18 were counted over each 4-hour sampling period. These raw particle counts were scaled using the scaling factors shown in Figure 5.1. These data

were plotted versus the mass loadings for the MOUDI impactors for ammonium ion mass concentration determined by ion chromatography (IC). A plot of this comparison is shown in Figure 5.3 below. Similarly, particles with an ion peak at mass/charge 30 were counted up over the same time period and scaled and plotted versus the nitrate mass loadings from the MOUDI impactors. This plot is shown in Figure 5.3 below.

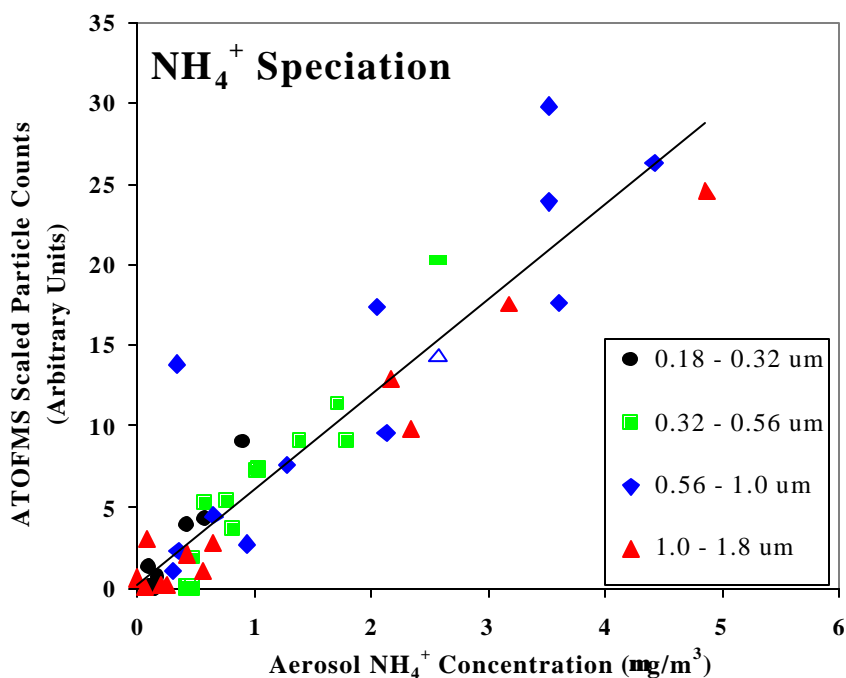


Figure 5.3: Comparison of scaled ATOFMS particle counts of particles containing ammonium (NH₄⁺) versus mass concentrations obtained on MOUDI filters sampled over a four hour time period.

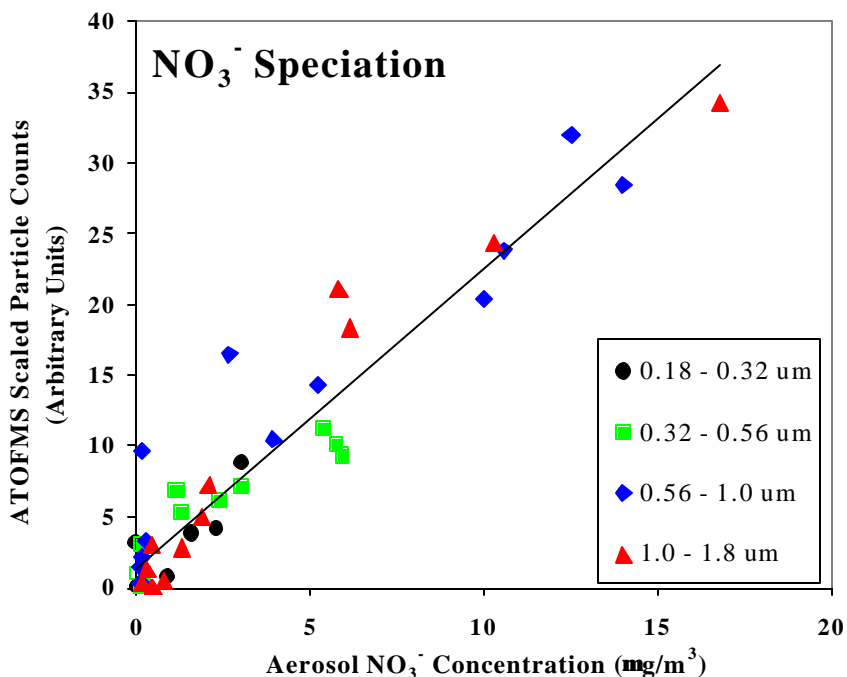


Figure 5.4: Comparison of scaled ATOFMS particle counts of particles containing nitrate (NO⁺) versus mass concentrations obtained on MOUDI filters sampled over a four hour time period.

Figures 5.3 and 5.4 show examples of comparisons between ATOFMS particle counts and MOUDI mass loadings for specific chemical species. These initial results show a great deal of promise that ATOFMS number counts can be scaled to mass distributions for specific chemical species. Work is underway in our labs making determinations for other chemical species including metals such as Fe, V, Al, Na, K and other species including total C, elemental C, chloride, and sulfate.

5.4 Transmission efficiency of transportable instruments

The experiments described above are part of an initial effort to compare ATOFMS data with MOUDI impactor data. As a first attempt, the results are quite promising. However, in being required to group the ATOFMS particles into size bins to match those of the MOUDI,

potentially valuable information is being lost by not utilizing the ability of ATOFMS to precisely size the particles (i.e. to within 1%). In addition, by averaging particles in set size bins determined by the MOUDI cuts, single particle chemical information of different particle type may be averaged together.

With this in mind, a different approach was explored for comparing the MOUDI and ATOFMS results. The objective of the work described in this section is to determine the particle detection efficiencies of ATOFMS instruments for ambient aerosols by comparison with more conventional reference samplers. The data used for comparison are the same data described previously in this report. The goal is to use aerosol mass distributions measured using co-located impactors for comparison against ATOFMS number counts acquired over the same time period to obtain the particle detection efficiencies of the ATOFMS instruments as a function of particle size. These detection efficiencies don't require grouping of ATOFMS particles into certain size cuts. However, if one chooses to for the sake of comparison, one can group the particle into any desired size cuts that are necessary. Using these detection efficiencies, we will determine aerosol mass concentrations from scaled ATOFMS data for the entire sampling period. Ultimately, we will establish how these scaled continuous aerosol mass concentrations compare with data obtained with optical particle counters.

5.5 Experimental

In order to compare the ATOFMS with a quantitative reference method, two MOUDI were used as primary reference samplers at each of the three sampling sites at the times discussed earlier. Additional reference sampling methods used during this study include inertial impactors, an optical particle counter, and an electric aerosol analyzer. AHIL-design cyclone impactors were used upstream of the MOUDI impactors in order to remove particles greater than

1.8 μm . Each impactor contains 10 stages with one impactor using aluminum substrates and the impactor containing Teflon substrates. Impactor stages 5-8 were used for comparison with ATOFMS data in this study, corresponding to size cuts of 1.0-1.8 μm , 0.56-1.0 μm , 0.32-0.56 μm , and 0.18-0.32 μm , respectively. No coatings were applied to minimize contamination. From previous studies, it has been shown that Los Angeles area fine particles are primarily aqueous or liquid organic coated, thereby making adhesive unnecessary. The substrates were weighed both prior to and after sampling on a mechanical microbalance (Mettler Model M-55-A) with 10 μg precision in a temperature and humidity controlled room.

Mass measurement of cascade impactor samples is the most direct method to determine aerosol mass distributions. MOUDI mass data are particularly useful for the calibration of ATOFMS counting efficiencies because both impactors and ATOFMS instruments segregate particles based on their aerodynamic diameters and operate over the same aerodynamic size range, approximately 0.1-2 μm . The aerosol mass concentration measured for a sample collected on stage i of a cascade impactor is designated m_i . This is deemed to be an accurate measure of the mass of particles between the upper and lower cut-off diameters of the impactor stage. Data from the optical particle counters (OPC) were not used as the primary reference data set because the relationship between particle size and light scattering intensity has been shown to depend on chemical composition, making the conversion between light scattering intensity and aerodynamic diameter difficult for atmospheric particles.

Over the period of the study, the three ATOFMS instruments sized 3.1×10^6 particles and collected mass spectra for 3.1×10^5 of these particles. Due to dispersion of the particle beam after the sizing region, only between 10-30% of the sized particles also get “hit” by the LDI Nd:YAG laser, producing a mass spectrum. Velocity and sampling time data were recorded for

each of the sized particles. Particle aerodynamic diameters, D_a , were determined from laboratory calibration curves that relate particle velocity to D_a as described in Chapter 2. From these data, the apparent aerosol number concentration in a particle size range j , n_j^* , is calculated as the sum of particles counted by an ATOFMS in the size range $D_{a,j} < D_a < D_{a,j+1}$ divided by the volume of air sampled. The size range of particles included in each ATOFMS size bin, j , can be conveniently chosen so that an integral number of narrower ATOFMS bins fit within each impactor, i .

If particles are assumed to be spherical and of uniform density, the apparent aerosol mass concentration in a particle size bin j , m_j^* , is

$$m_j^* = n_j^* \frac{\rho_p}{6} r_p \overline{D_{p,j}^3} \quad (5.1)$$

where ρ_p is the particle density and $\overline{D_{p,j}^3}$ is the logarithmic mean average particle diameter in size bin, j . Here each impactor bin, i , is divided into 10 ATOFMS size bins, j . The ratio of the upper to lower particle size limit for each of these bins is approximately 1.06, which is sufficiently small so that $\overline{D_{p,j}^3}$ is an accurate representation of particles in each size bin.

Equation 5.1 is more conveniently expressed in terms of the average aerodynamic diameter $\overline{D_{p,j}^3}$. The relation between D_p and D_a is

$$D_p = D_a \left(\frac{r_1 C_c(D_a)}{r_p C_c(D_p)} \right)^{1/2} \quad (5.2)$$

where ρ_p is unit density (1 g/cm^3) and C_c is the slip correction factor for flow in the transition regime. The aerosol mass density is assumed to be 1.7 g/cm^3 . This is a common assumption used for the density of atmospheric particles; however, with future ATOFMS measurements, we will be able to determine the density of the particle more directly since single particle

composition is measured directly. For the purposes of this particular study, it was assumed all particles have the same density of 1.7. For particles with $D_a > 0.1 \mu\text{m}$, the ratio in Equation 5.2 is less than 1. Therefore, the slip correction may be ignored and Equation 5.2 becomes

$$m_j^* = n_j \frac{\rho r_1^{3/2}}{6r_p^{1/2}} D_{a,j}^3 \quad (5.3)$$

Apparent aerosol mass concentrations may then be compared with data from reference method samplers.

A measure of the particle detection efficiency of an ATOFMS is the ratio of aerosol mass as measured with an impactor to that estimated from ATOFMS number count data, ϕ , calculated as

$$f = \frac{m_i}{\sum_{j \in i} m_j^*} \quad (5.4)$$

Note that ϕ is the inverse of the particle detection efficiency. For the transportable instruments, ϕ is in the range 10^1 to 10^5 for particles with $0.32 < D_a < 1.8 \mu\text{m}$ as shown in Figure 5.5. Data for the two transportable instruments operated in Long Beach and Fullerton are plotted together since, within the precision of the experiment, the data are indistinguishable. This is expected since these units have the same design and were constructed to be “identical”. Values of ϕ show a strong dependence on D_a ; a smaller fraction of small particles are detected. The dependence of $\log\phi$ on $\log D_a$ is approximately linear.

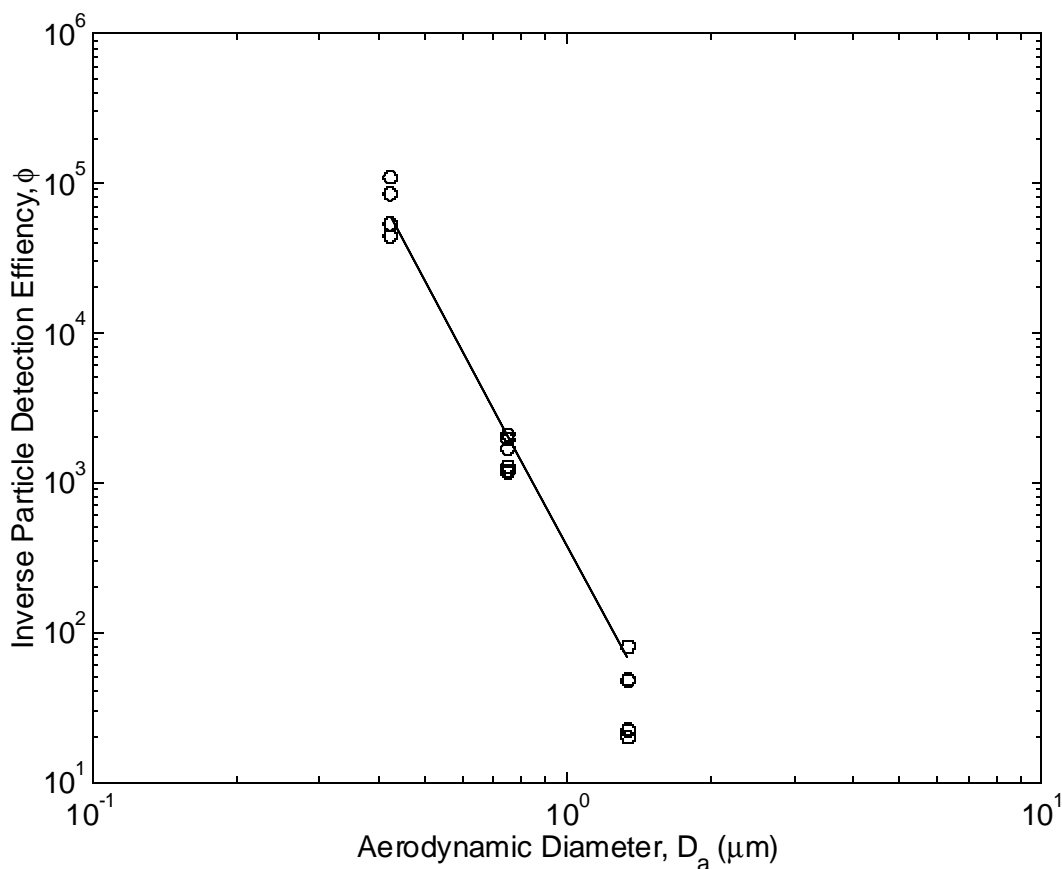


Figure 5.5: Inverse particle detection efficiency (ϕ) versus aerodynamic diameter (D_a) for the transportable ATOFMS instruments during sampling in Long Beach and Fullerton.

The relative steepness of the curve in Figure 5.5 shows there is a substantial falloff in detection efficiency for smaller particles. The slope of the curves is much steeper than that for the lab-based ATOFMS system. This discrepancy caused us to examine the reason for the observed differences after the study. It was determined that the primary reason for these losses was due to transmission problems due to the two chosen distances between the nozzle and first skimmer and the second and third skimmer. These distances have now been adjusted to optimize particle transmission for smaller particles, so they are detected more efficiently. This will cause the slope of the fit in Figure 5.5 to decrease substantially. It is important to note that

the unique adjustability of these distances in the interface of the ATOFMS instruments made this improvement possible.

It is important to note that the sampling biases of the transportable ATOFMS instruments are advantageous for the accurate determination of aerosol concentration and chemical composition. This is because the portable ATOFMS instruments at typical atmospheric concentrations count and size approximately 2 particles per second and hit approximately 10% of the sized particles. For a typical urban aerosol, the number concentration of accumulation mode particles ($0.1 < D_p < 2.0 \mu\text{m}$) is approximately 10^3 cm^{-3} . In addition, number distributions for accumulation mode aerosols show an approximately logarithmic increase in the number of particles as the particle size decreases. Approximately 2×10^4 accumulation mode particles are introduced into the ATOFMS each second and the vast majority of these particles have sizes toward the lower limit of the detectable particle size range. Because only a small fraction of the sample aerosol particles can be sized and hit by ATOFMS, if particle sampling were not strongly biased against detecting smaller particles, only the more numerous smaller particles would be detected. Ideally, particles should be sampled to provide a good representation of the aerosol across all particle sizes. Thus, sampling should be biased so that the likelihood of a particle being sampled is proportional to its contribution to the target distribution. For accurate determination of the aerosol number concentration, the sampling bias should be proportional to D_a^{-1} whereas for mass concentration, the bias should be proportional to D_a^{-3} .

The objective of this work is to determine the counting efficiencies of the ATOFMS instruments by comparison with reference method data. We hypothesize that the ATOFMS particle size data can be reliably scaled by ϕ to yield atmospheric aerosol mass concentrations. This hypothesis can be expressed as a testable model by rearrangement of Equation 5.4 to

$$m_i = \sum_{j \in C_i} j m_m^* + \epsilon \quad (5.5)$$

where ϵ is the residual aerosol mass concentration not accounted for in the model.

The observation that particle counting efficiencies are strongly dependent on particle size is consistent with particle losses being dominated by transmission losses through the interface. The observed power law dependence of counting efficiency on particle size is like that observed for transmission through nozzles (Dahneke and Cheng 1979). Based on these observations, we make the *a priori* assumption that particle counting efficiency is primarily dependent on particle size.

Plots of ϕ versus D_a suggest that ϕ follows a power law relationship in D_a (see Figure 5.5). With this functional form for ϕ , Equation 5.5 becomes

$$m_i = \sum_{j \in C_i} a D_a^b m_j^* + \epsilon \quad (5.6)$$

Parameters a and b were determined by nonlinear regression analyses separately on the data from the transportable and laboratory ATOFMS instruments. Nonlinear regression analyses were performed according to the method of Bates and Watts as implemented in the Matlab statistics package (Mathworks, Natick, MA). Fitted values of a and b are 383 ± 182 and -5.85 ± -1.36 , respectively. The fitted scaling functions are shown as a line in Figure 5.5.

We have assumed that the scaling factor, ϕ , is not affected by particle composition. A test of this assumption can be made by examining the correlation of residuals from Equation 5.6 with other variables. Extensive aerosol composition data are available from analyses of the impactor samples collected during the intensive sampling times. The residuals were uncorrelated with aerosol concentrations of elemental carbon, organic carbon, ammonium, nitrate, sulfate, sodium, magnesium, and other detected species.

One application of the scaling functions developed from data for the intensive sampling periods is to use the ATOFMS data to estimate the aerosol concentrations over the entire study period. The scaling functions can be used to estimate the continuous aerosol mass concentration with particle size resolution as

$$\hat{m}_i = \sum_{j \in i} a_j D_j^b m_j^* \quad (5.7)$$

where \hat{m}_i is the estimate of the aerosol mass concentration in particle size bin i . Confidence intervals as \hat{m}_i can be made if the estimates have the same time and particle size averaging as m_j , i.e. MOUDI particle size bins with 4 hour averaging times.

Fine aerosol mass concentrations are estimated from ATOFMS data for the entire study period in Long Beach. Shown in Figure 5.6 are the data for the 0.32-0.56 μm and 0.56-1.0 μm size bins. Scaled ATOFMS data are the solid lines with gray areas showing 95% confidence intervals. OPC data are the dashed line and the points are the MOUDI data with error bars showing a 95% confidence interval. Data from the Fullerton site are not shown since ATOFMS data are available for only 48 h and the comparisons are similar to those from the Long Beach site.

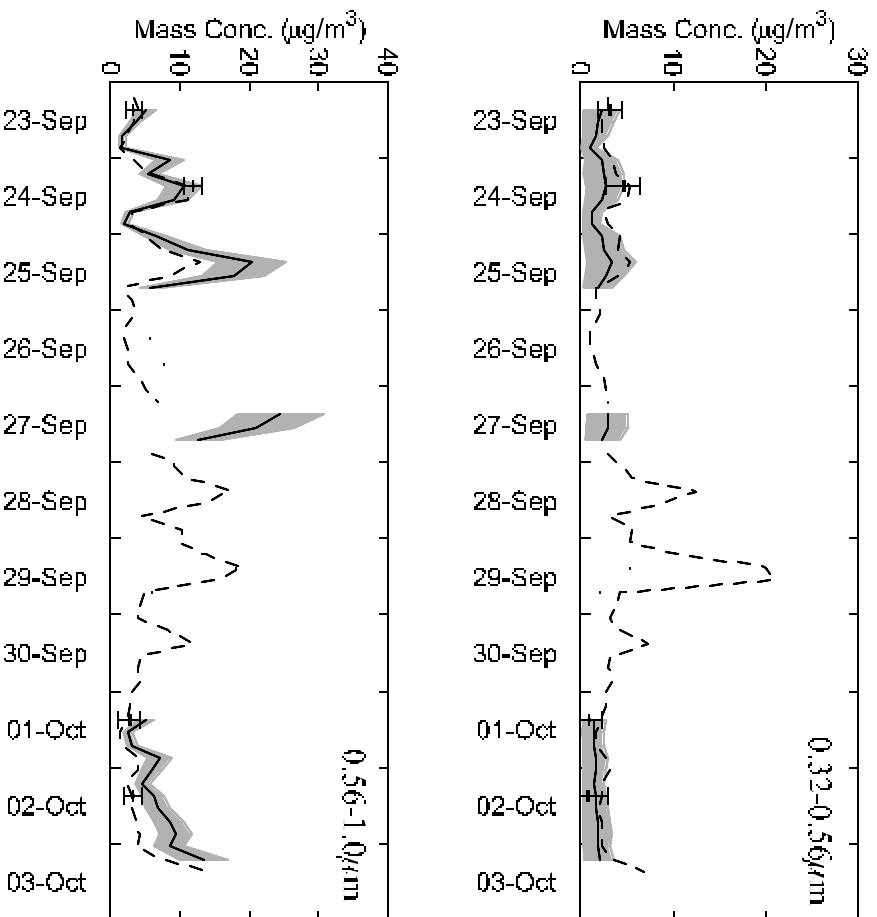


Figure 5.6: Continuous fine aerosol mass as determined from the ATOFMS, impactor, and optical particle counter at Long Beach from September 23 through October 2, 1996.

A comparison of the scaled ATOFMS and impactor data show that these data match well during most of the intensive sampling events. The general agreement between the scaled ATOFMS and impactor data indicates that the chosen scaling function accurately represents the performance of the transportable ATOFMS instruments during the intensive sampling events carried out over the entire course of the field experiment.

The reconstruction of continuous time series aerosol mass concentration data from

ATOFMS data is a useful but limited result. In addition to particle size data, ATOFMS instruments record the mass spectra of single particles. One can apply the ambient particle detection scaling function developed here to estimate the number of particles of a given composition in ambient aerosols. The first efforts to do this are underway and discussed in the following section.

5.6 Quantitation of individual species

In order to determine chemical composition mass concentrations from the ATOFMS data, marker peaks were searched for in each individual particle “hit” in each of the six 4 hour intensive sampling time periods. Search criteria for a particle with a given chemical species include mass peaks with a given mass/charge and relative peak area (RA). RA can be defined in the search program from a range of 0 to 1, indicating a range of 0 to 100%. In addition, search criteria can be tailored to use “and”, “or”, and “union” statements when searching for particle containing combinations of two or more marker peaks. This allows for the possibility of excluding particles that have mass peaks known to be associated with chemical species that generate ions that interfere with the desired marker peak.

Particles containing marker peak(s) with a relative area above the defined search criteria are called selected “hits”. The particles selected are then individually scaled using the equation:

$$SC = RA * aD_a^b \quad (5.8)$$

where SC are the scaled counts corrected for transmission efficiency, D_a^b is the scaling equation discussed in the last section, and RA is the relative area of the marker peak(s). The same equation is applied to total “hits” and “misses” using a simplified form:

$$SC = aD_a^b \quad (5.9)$$

The selected “hit” particles are then separated individually into size bins that are the same as the

impactor stage size cuts. Total “hits” and “misses” particles are also size sorted individually into size bins in the same manner as the selected “hits” mentioned above. Missing time (MT) is determined in another subroutine of the MATLAB program. MT is an interpolation of total “hits” and “misses” when it is determined that there are time period gaps where no data was collected, and MT is proportional to the extent of time that is missing. This correction is necessary for down sampling periods due primarily to cleaning the ATOFMS nozzle inlet and other maintenance procedures. Following size sorting, a ratio of selected “hits” to total “hits” is calculated for each size bin and then used to determine the total selected “hits” by multiplying the total number of particles (“hits” + “misses” + MT) in a size bin times the ratio determined by selected the ratio of “hits”/total “hits”.

As discussed previously, in order to obtain size and chemically resolved particle number counts with the ATOFMS instrument, it is necessary to find peaks in the mass spectra that are indicative of a specific chemical species present in the particle. It is important to find marker peaks for a given species that doesn't interfere with the chemical signature of another species also present in the particles. For example, for the ammonium ion (NH_4^+) as shown in Figure 2.7, the chosen marker is the ion peak at mass-to-charge 18. We have found in lab studies running particles of ammonium nitrate that this is an appropriate marker. There may also be some amount of 18 present in a particle composed of nitrogen containing organic compounds, but the relative amount of ion intensity in atmospheric particles is small compared to that for ammonium. The marker for nitrate is mass/charge 30, corresponding to NO^+ which forms when laser desorption/ionization of NH_4NO_3 takes place. Again, by running lab studies, it is believed there will be minimal interference from other ions at m/z 30.

Once ATOFMS data have been corrected, they may be plotted versus the chemical

species mass concentration obtained for each of the intensive periods from the impactor stages, plotting each size bin individually. Figure 5.7 shows the calibration for nitrate (NO^+) plotted for the 0.56-1.0 μm size bin. The x-axis is represented by the mass concentration of nitrate obtained from impactor sample analysis of nitrate in the 0.56-1.0 μm size bin and the y-axis is the scaled counts (SC) for the ATOFMS with mass/charge 30 as the marker ion for all particles with sizes between 0.56 and 1.0 μm . Similar results were obtained when NH_4^+ is plotted versus counts containing the marker mass/charge.

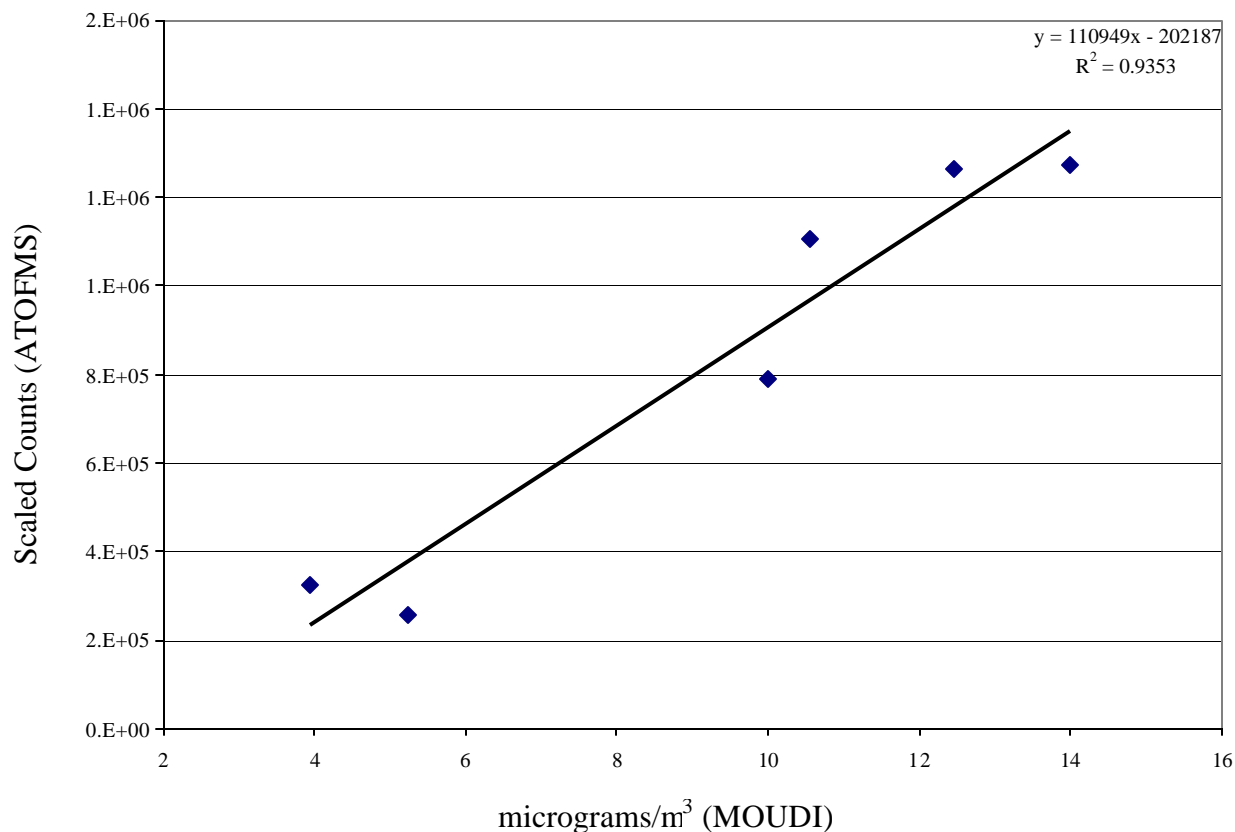


Figure 5.7: Calibration curve showing the scaled counts (SC) of the ATOFMS (y-axis) versus the mass concentration of nitrate from the 0.56-1.0 mm size bin of the MOUDI.

The ATOFMS was run continuously over the study even when the impactors were not being run. Data obtained outside the intensive sampling periods are handled in an identical manner to the data compared directly to impactor mass concentrations. A linear least squares

regression is performed to obtain a calibration curve that can be applied to quantify ATOFMS data that was collected outside the intensive sampling periods. Comparisons of the ATOFMS data obtained in this manner with MOUDI data are shown for nitrate and ammonium in Figures 5.8 and 5.9, respectively. One can see that the six MOUDI points in each plot compare well with the scaled ATOFMS data at the sampling times indicated by the vertical arrows and horizontal bars, showing the feasibility of this method of calibration.

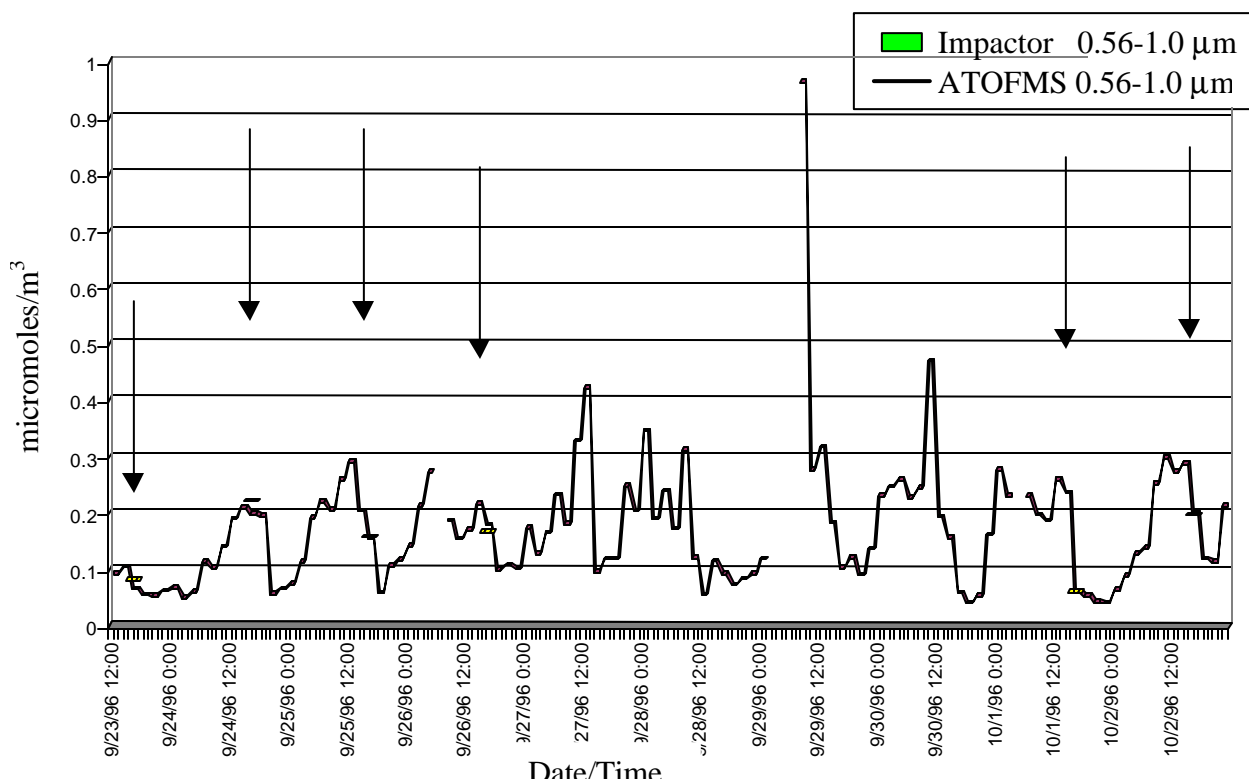


Figure 5.8: Comparison of calibrated ATOFMS data with mass concentration of nitrate collected in the 0.56-1.0 mm size bin of the MOUDI impactor on six different days in Riverside.

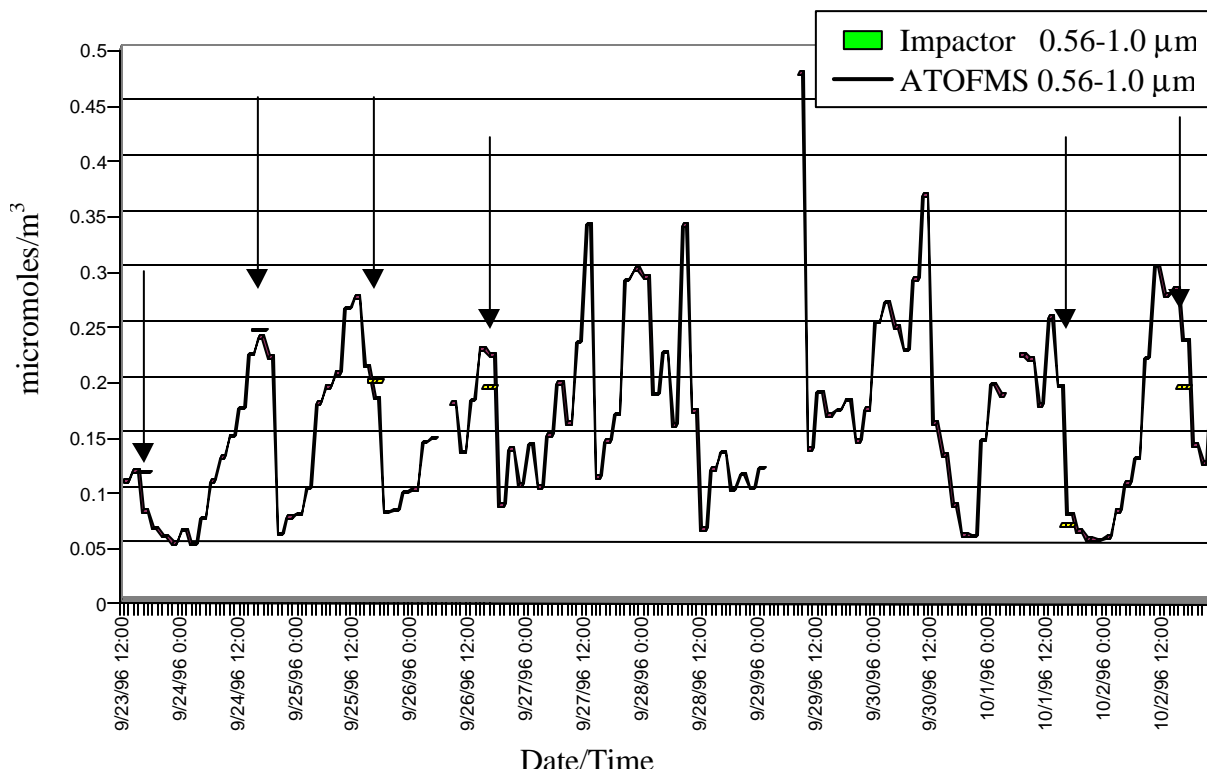


Figure 5.9: Comparison of calibrated ATOFMS data with mass concentration of ammonium collected with MOUDI impactors on six different days in Riverside.

5.7 Laboratory quantitation studies

Another approach for calibrating the ATOFMS instruments involves creating particles in the laboratory of known size and composition. If one knows the concentration of the species of interest in the particles, then one can directly determine the sensitivity of ATOFMS for various species. This information combined with studies which measure the transmission and detection efficiency of the ATOFMS instruments will allow for direct determination of the necessary scaling factors to convert the raw atmospheric data into representative values. These studies are currently being conducted in our laboratory. After the lab studies are complete, we intend to determine whether the results obtained in the lab compare well with those obtained as part of this project, involving the measurement of ambient particles in the field. It is important to note that

results from lab and field studies can provide complementary information. In the lab, it is nearly impossible to replicate atmospheric conditions and concentrations of polydisperse and heterogeneous particles. On the other hand, in the field one has to accept that there are more unknowns and in general one has less control of multiple parameters. Given that neither option offers the “perfect” solution, the approach that we are taking with our new ATOFMS instruments is to try both approaches (i.e. lab and field measurements) allowing for direct comparison of the results.

A variety of analytical techniques rely on the use of relative sensitivity factors (RSF’s) for obtaining quantitative or semiquantitative results from multi-component samples. These factors correct for differences in the response of the various species to the method being used, as well as for changes in the response of a particular species due to changes in the sample matrix. These RSF’s are empirically determined, based on Equation 5.10,

$$RSF\left(\frac{A}{B}\right) = \frac{n_i^A / n_a^B}{n_a^A / n_a^B} \quad (5.10)$$

where n_i^X and n_a^X refer to the number of ions and atoms, respectively, of species X present.

In studies aimed at determining the relative response for various chemical species in individual particles, a monodisperse aerosol is generated using a vibrating orifice aerosol generator (VOAG) (TSI, Inc., Cincinnati, OH). In initial studies, salt solutions were made from NaCl and KCl (Sigma Chemical Company, St. Louis, MO), diluted in 50/50 methanol/water (by volume). Solution concentrations were used which would generate particles with aerodynamic diameters of ~0.8 μm , and are shown in Table 5.1, along with the average number of moles of

Table 5.1. Concentrations of Na⁺ and K⁺ ions in the eight solutions used in this study. The solutions are mixtures of only NaCl and KCl, in 50/50 methanol/water (by volume). Also included is the average number of moles of each cation per single-mode particle measured here.

Solution	Na ⁺ /K ⁺ (solution)	[Na ⁺] (mM)	[K ⁺] (mM)	Moles Na ⁺ /particle (x 10 ⁻¹⁵ moles)	Moles K ⁺ /particle (x 10 ⁻¹⁵ moles)
1	0.5	25.7	48.3	0.45	0.90
2	1.0	38.5	36.9	1.26	1.26
3	5.1	68.4	13.4	1.29	0.25
4	9.0	75.3	8.4	1.27	0.14
5	14.7	78.7	5.4	1.44	0.10
6	18.4	80.0	4.4	1.68	0.09
7	30.5	81.8	2.7	1.41	0.05
8	38.6	82.8	2.2	1.33	0.03

each cation in the particle. In addition to these single ~0.8 μm particles, larger particles were also observed, in which two and three particles coalesced (*i.e.* doublets and triplets, respectively). It is evident from the mass spectra of particles formed from a solution containing known concentrations of sodium and potassium that the instrumental response to these cations is not identical. Figure 5.10 shows single-particle mass spectra of particles formed from solutions 2 and 8 (Table 5.1). Each spectrum results from a single laser-shot interacting with a single particle. Evident in these spectra are peaks corresponding to Na⁺ and K⁺, as well as the cluster ions K₂Cl⁺ and Na₂Cl⁺, from solutions 2 and 8, respectively. These clusters, as well as mixed clusters such as NaKCl⁺, were observed in a number of the particles formed from each of the solutions. No other ions were present in the mass spectra. Clearly the ratio of the relative

intensity of the cation signals does not directly reflect the solution ratios. In order to obtain an

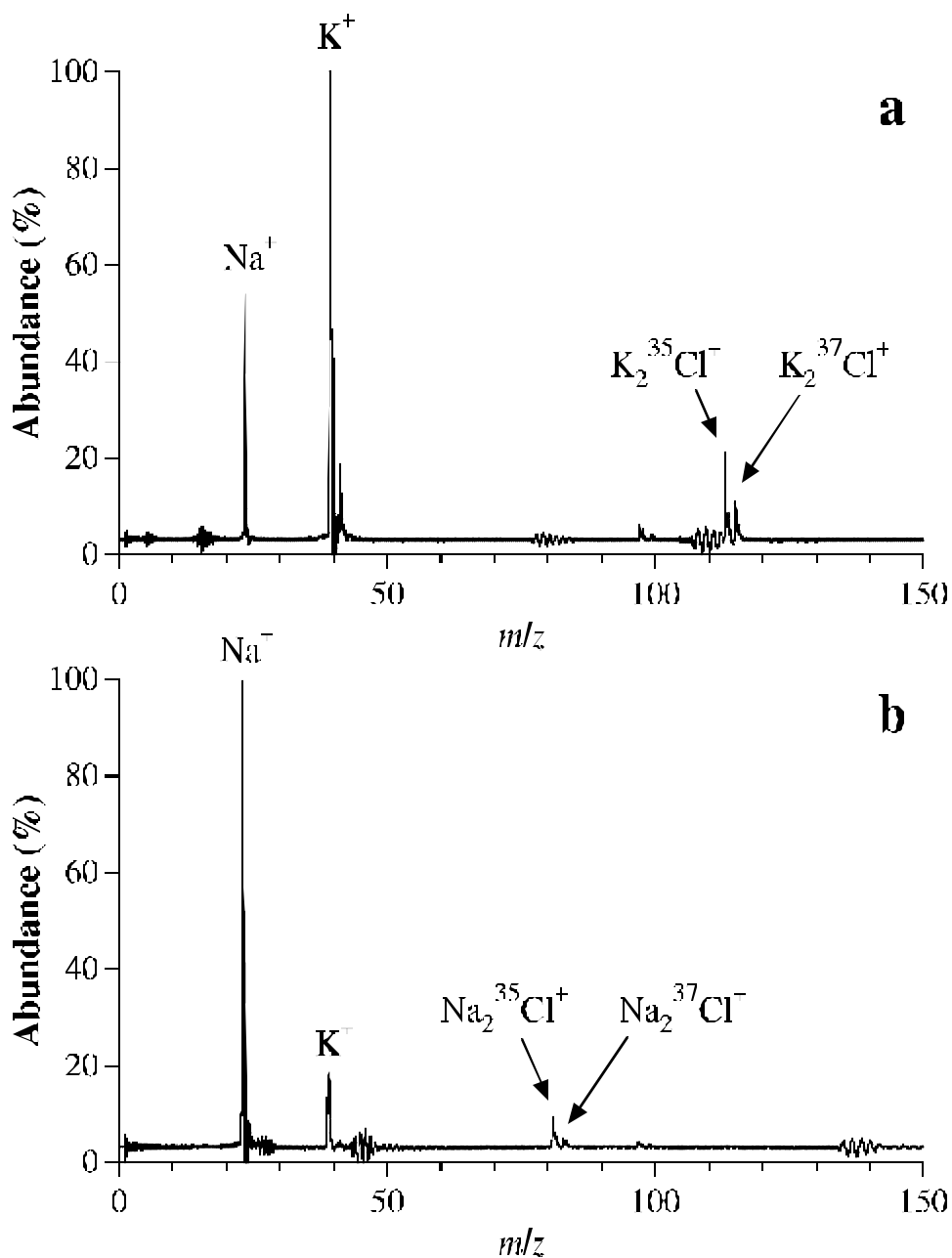


Figure 1.

Figure 5.10: Time of flight mass spectra of individual particles formed from a) solution 2 ($\text{Na}^+/\text{K}^+ = 1.0$) and b) solution 8 ($\text{Na}^+/\text{K}^+ = 38.6$). Atomic ions as well as clusters with the Cl^- counterion are labeled. Each spectrum is the result of a single laser shot interacting with a single particle.

RSF which can be used to determine the relative amounts of these cations in an ambient particle, we measured the relative sensitivity factor of these ions over the widest possible range of salt concentrations. Solutions 1 and 8 have concentrations very near the detection limits of Na^+ and K^+ , respectively, implying that the detection limits for these species are ~ 0.45 and 0.03×10^{-15} moles, respectively (see Table 5.1).

Figure 5.11 shows the relative area of Na^+ versus K^+ for all 8 solutions. The clusters of the relative area of these cations for each solution overlap somewhat, however there is a clear progression from solution 8, with the highest relative intensity of K^+ , to solution 1, with the highest relative intensity of Na^+ . The variation is dramatically less than that in the absolute areas of the same peaks. Table 5.2 gives the average and standard deviation of the absolute and relative peak areas for the single-mode particles measured. Relative peak area is obtained

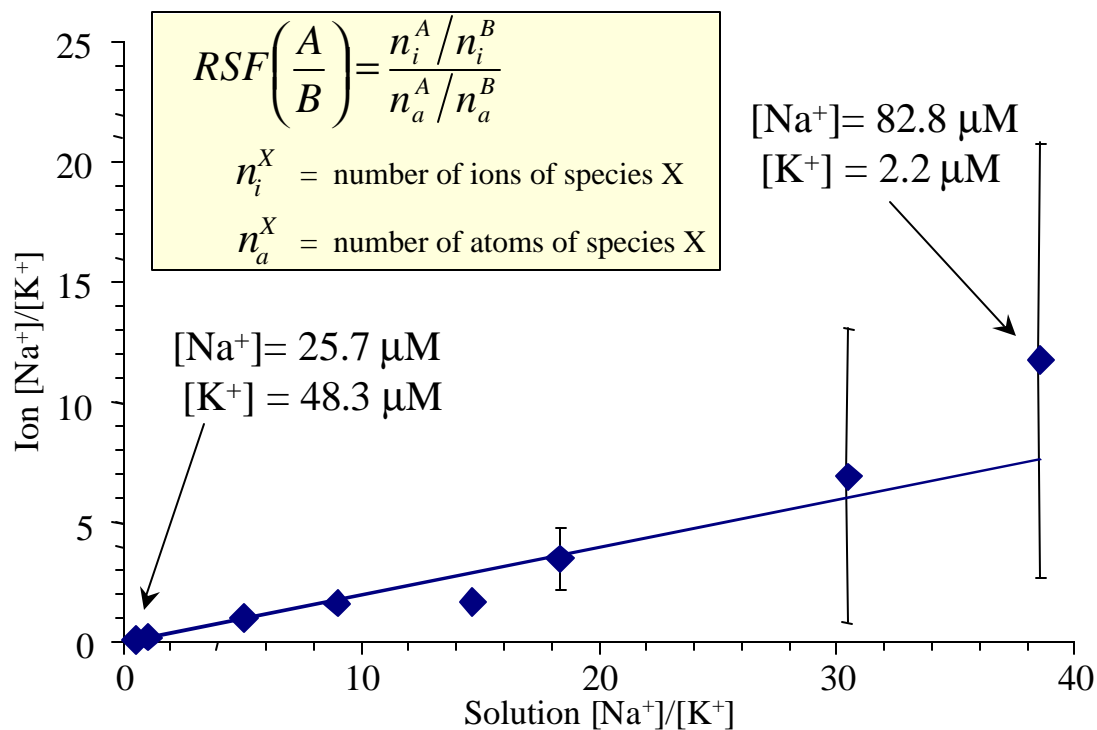


Figure 5.11: Plot of Na^+/K^+ ion ratio versus solution ratio for 8 monodisperse particles

types. Each point represents the average of the ratios of 200 - 400 individual particles.

by taking the absolute area of the ion peak of interest and dividing it by the total area of all ion peaks in the mass spectrum. The decrease in scatter of the relative ion peak area occurs because factors such as particle-ionization laser interactions, laser power, and any other variables which affect the total area in each spectrum, are normalized out. This demonstrates that the relative peak areas determined from single-particle mass spectra are directly comparable, without the need for averaging multiple spectra. This is an important factor for studies aimed at being quantitative of heterogeneous aerosol particles, where one doesn't want to average particles of mixed composition and lose single particle information. A comparison of the ratio of the relative area of any peaks within an individual spectrum to the ratio of the same peaks in another spectrum will provide relative quantitation to within ~10 - 20 %.

Table 5.2. Average and standard deviation of absolute and relative peak areas of Na⁺ and K⁺ ions formed from the laser-desorption of individual aerosol particles formed from solutions 1 through 8.

Solution	Na ⁺ Peak Area		K ⁺ Peak Area	
	(Absolute)	(Relative)	(Absolute)	(Relative)
1	979 ± 1486	0.076 ± 0.092	12847 ± 14478	0.718 ± 0.113
2	1411 ± 833	0.152 ± 0.047	5544 ± 2252	0.688 ± 0.085
3	3138 ± 1519	0.448 ± 0.055	3091 ± 1371	0.453 ± 0.041
4	4287 ± 1711	0.541 ± 0.055	2799 ± 1242	0.346 ± 0.036
5	4321 ± 1775	0.589 ± 0.070	2168 ± 1048	0.283 ± 0.042
6	4372 ± 1703	0.663 ± 0.071	1539 ± 822	0.220 ± 0.048
7	3918 ± 1847	0.706 ± 0.073	905 ± 598	0.146 ± 0.040
8	4004 ± 1674	0.752 ± 0.067	580 ± 357	0.100 ± 0.030

In Figure 5.13, the resulting dual ion mass spectra are shown for a particle composed of a mixture of calcium chloride and sodium nitrate. Using the transportable instruments, one can measure the relative response for cations and anions, simultaneously. Note that in the mass spectrum on the right that the chloride ion intensity is higher than that for the nitrate. As shown in the inset, the particle actually contained more nitrate than chloride. Similar to the example of K^+ and Na^+ , this further demonstrates that relative ion intensity cannot be used as a direct indication of the amount of a particular compound is contained in a particle. One must obtain relative sensitivity factors.

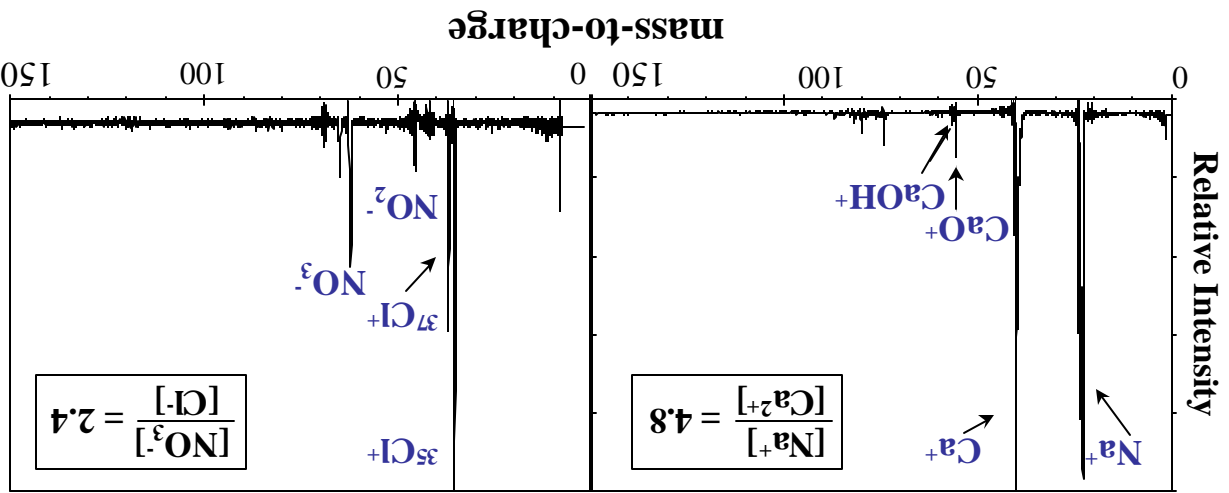


Figure 5.12: Dual ion polarity mass spectra of a single $CaCl_2/NaNO_3$ particle. The bulk ion ratios are shown in the figure.

Ongoing studies in our labs are continuing to focus on obtaining relative sensitivity factors for various chemical species expected to be found in atmospheric aerosols. In studies to date, we have examined the compounds listed in Table 5.3.

Table 5.3: Measured relative sensitivity factors for various ions in single particles analyzed to date by ATOFMS.

Ion Pair	RSF
Ca⁺/Na⁺	2.2
K⁺/Na⁺	5.1
NH₄⁺/Na⁺	0.014
Cl⁻/NO₃⁻	5.6

As shown in Table 5.3, studies to date have involved making measurements on particles composed of inorganic compounds. It is possible that the overall sensitivity to a particular compound may change for species in various matrices, i.e. sea salt versus organic particles. Thus, we are investigating the effects of varying the compositions of particles taking this into account. As one might imagine, this will take a tremendous amount of work.

Chapter 6

Current and Future Directions

The 1996 field experiment represents the first field study performed with ATOFMS. It has demonstrated that ATOFMS can provide semi-quantitative data when scaled with MOUDI impactor data and OPC data. In future studies, we plan to perform more side-by-side comparisons as well as complementary studies to determine how consistent the ATOFMS calibration parameters are from one study and/or location to the next.

These studies have allowed for comparisons between ATOFMS and a more standard aerosol sampling technique over a four hour time period. However, ATOFMS is a continuous aerosol analysis technique so a question exists as to how short a time scale ATOFMS can provide quantitative information. Recently, Hering et al. developed a real-time nitrate monitor (Hering and Stolzenburg 1998). In a side-by-side study conducted with Hering in SCOS97, we sampled ambient particles continuously. A comparison of the two methods is shown below. The nitrate data obtained with 10-minute temporal resolution are plotted as mass concentrations and the ATOFMS data are plotted as the number of particles containing nitrate (NO^+) over the same 10 minute time increments. The data are shown for a four-day period on August 21, 1998 – August 24, 1997 in Figure 6.1.

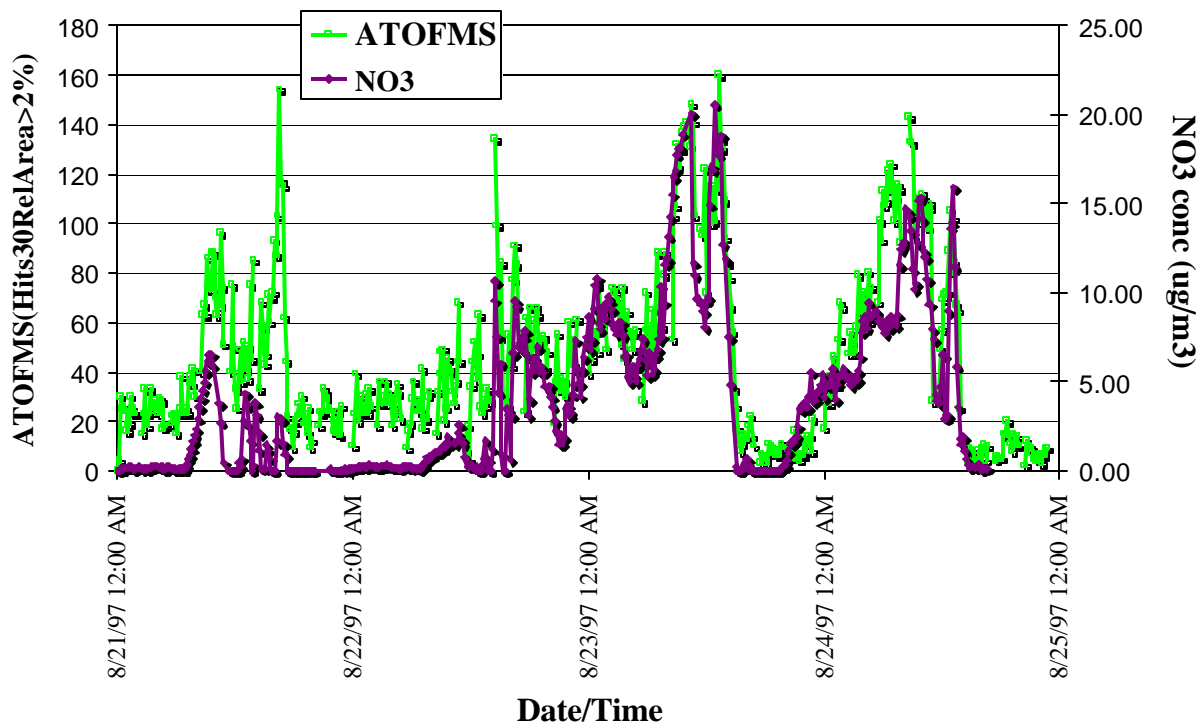


Figure 6.1: Comparison of nitrate measurements made by ATOFMS and another real-time nitrate monitor showing 10 minute temporal resolution.

This study represents a first attempt at comparing the ATOFMS data in its simplest possible form of number counts with another measurement method with high temporal resolution. At a first glance, it is somewhat surprising that number counts of ATOFMS matches nitrate mass so well. However, because of the inherent transmission efficiency of the ATOFMS systems, ATOFMS number distributions, as unscaled raw data, resemble mass distributions. This is a fortuitous result and primarily due to the transmission efficiency of the ATOFMS instruments which favors particles greater than 1 μm in diameter which is where the majority of particle mass occurs. Therefore, with this in mind, it is not a complete surprise that the number counts match the nitrate mass measurements over time. Ultimately, we will take into account the

relative intensity of the marker peaks of the nitrate in the mass spectra of the particles but as a first attempt, these results are extremely exciting. They are promising from two important standpoints; these results indicate ATOFMS measurements of aerosol processes can be made with temporal resolution down to 10 minutes if adequate ambient aerosol concentrations exist. They also show that raw ATOFMS data as they are acquired can be used to obtain rapid information on the aerosol particles occurring in the atmosphere.

Currently, we are working on finishing the quantification of various species for the three instruments. In addition, we are comparing our single particle results with those predicted by the external mixture model of Kleeman and Cass for various parts of the field study. A major focus will be to examine how individual particles evolve as they move inland through areas of high pollution. Meteorological data indicate that a trajectory in the first part of the study passed through all three monitoring sites. In addition to further field work, we are continuing in our efforts to calibrate the instruments for transmission efficiency and chemical sensitivity by performing additional lab studies which will be compared with the results obtained in the field. Most recently, the data from the 1996 field study were used to obtain promising results on the ability to perform a multivariate calibration of the ATOFMS data with the MOUDI impactor, quantifying 44 species simultaneously (Ferguson, D. P. et al. 2001).

References

- Allen, J. O., D. P. Fergenson, E. E. Gard, L. S. Hughes, B. D. Morrical, M. J. Kleeman, D. S. Gross, M. E. Gaelli, K. A. Prather, G. R. Cass (2000). "Particle Detection Efficiencies of Aerosol Time-of-Flight Mass Spectrometers Under Ambient Sampling Conditions." Environ. Sci. Technol. **34**: 211.
- Beichert, P. and B. J. Finlayson-Pitts (1996). "Knudson Cell Studies of the Uptake of Gaseous HNO₃ and Other Oxides of Nitrogen on Solid NaCl: The Role of Surface Absorbed Water." J. Phys. Chem. **100**: 15218.
- Bruynseels, F. and R. Van Grieken (1985). "Direct Detection of Sulfate and Nitrate Layers on Sampled Marine Aerosols by Laser Microprobe Mass Analysis." Atmos. Environ. **19**: 1969.
- Carson, P. G., K. R. Neubauer, et al. (1995). "Online Chemical Analysis of Aerosols by Rapid Single-Particle Mass Spectrometry." J. Aerosol Sci. **26**: 535.
- Dahneke, B. E. and Y. S. Cheng (1979). "Properties of Continuum Source Particle Beams. I. Calculation Methods and Results." J. Aerosol Sci. **10**: 257.
- Dockery, D. W. and C. A. Pope (1994). Ann. Rev. Public Health **15**: 107.
- Eldering, A. and G. R. Cass (1996). "Source-Oriented Model for Air Pollutant Effects on Visibility." J. Geophys. Res. **101**, 343.
- Fergenson, D. P., X-H. Song, Z. Ramadan, J. O. Allen, L. Hughes, G. R. Cass, P. K. Hopke, K. A. Prather (2001). "Quantitation of ATOFMS Data Using Multivariate Methods." Anal. Chem. **73**, 3535.
- Finlayson-Pitts, B. J. and J. N. Pitts Jr. (1986). Atmospheric Chemistry: Fundamentals and Experimental Techniques. New York, Wiley.
- Gaelli, M., S. A. Guazzotti, K. A. Prather (2001). "Improved Lower Particle Size Limit for Aerosol Time-of-Flight Mass Spectrometry." Aerosol Sci. Technol. **34**: 381.
- Gard, E., J. E. Mayer, et al. (1997). "Real-Time Analysis of Individual Atmospheric Aerosol Particles: Design and Performance of a Portable ATOFMS." Anal. Chem. **69**: 4083.
- Godleski, J. (1998). Physics and Chemistry of Fine Particles. American Association for Aerosol Research (AAAR), Cincinnati, OH.
- Gross, D., M. Gaelli, et al. (2000). "Relative Sensitivity Factor for Na⁺ and K⁺ Ions in Single-Particle Aerosol Time-of-Flight Mass Spectra." Anal. Chem. **72**: 416.
- Hinz, K.-P., R. Kaufmann, et al. (1994). "Laser-Induced Mass Analysis of Single Particles in the Airborne State." Anal. Chem. **66**: 2071.
- Hughes, Lara S., J. Allen, M. J. Kleeman, R. Johnson, G. R. Cass, D. S. Gross, E. E. Gard, M. Gaelli, B. Morrical, D. Fergenson, T. Dienes, C. Noble, D. Liu, P. Silva, K. A. Prather (1999). "The Size and Composition Distribution of Atmospheric Particles in Southern California." Environ. Sci. Technol. **33**: 3506.

- Hughes, L.S.; J. O. Allen, P. Bhave, M.J. Kleeman, G.R. Cass, D.-Y. Liu, D. Fergenson, B. Morrical, K. A. Prather (2000). "Evolution of Atmospheric Particles Along Trajectories Crossing the Los Angeles Basin." Environ. Sci. Technol. **35**: 3058.
- Johnston, M. V. and A. S. Wexler (1995). "MS of Individual Aerosol Particles." Anal. Chem. **67**: 721A.
- Kleeman, M. J., G. R. Cass, et al. (1997). "Modeling the Airborne Particle Complex as a Source-Oriented External Mixture." J. Geophys. Res. **102**: 21355.
- Langer, S., R. Pemberton, et al. (1997). J. Phys. Chem. **101**: 1277.
- Leu, M.-T., R. S. Timonen, et al. (1995). "Heterogeneous Reactions of $\text{HNO}_3(\text{g}) + \text{NaCl}(\text{s})$, $\text{HCl}(\text{g}) + \text{NaNO}_3(\text{s})$ and $\text{N}_2\text{O}_5(\text{g}) + \text{NaCl}(\text{s})$, $\text{ClNO}_2(\text{g}) + \text{NaNO}_3(\text{s})$." J. Phys. Chem. **99**: 13203.
- Liu, D.-Y., D. Rutherford, et al. (1997). "Real-Time Monitoring of Pyrotechnically Derived Aerosol Particles in the Troposphere." Anal. Chem. **69**: 1808.
- Liu, D. -Y., S. Hering, and Kimberly A. Prather (2000). "Variations in Nitrate Containing Particles in Riverside, CA." Aerosol Sci. Technol. **33**:71.
- Mamyrin, B. A. (1994). "Laser Assisted Reflectron Time-of-Flight Mass Spectrometry." Inter. J. of Mass Spec. Ion Proc. **131**: 1.
- Molina, M. J. (1996). Angew. Chem. Int. Ed. Engl. **35**: 1778.
- Murphy, D. M. and D. S. Thomson (1997). "Chemical Composition of Single Aerosol Particles at Idaho Hill: Positive Ion Measurements." J. Geophys. Res. **102**: 6341.
- Noble, C. A. and K. A. Prather (1996). "Real-Time Measurement of Correlated Size and Composition Profiles of Individual Atmospheric Aerosol Particles." Environ. Sci. and Technol. **30**: 2667.
- Prather, K. A., T. Nordmeyer, et al. (1994). "Real-Time Characterization of Individual Aerosol Particles Using Time-of-Flight Mass Spectrometry." Anal. Chem. **66**: 1403.
- Pszenny, A. et al. (1993). Geophys. Res. Lett. **20**: 699.
- Ravishankara, A. R. (1997). "Heterogeneous and Multiphase Chemistry in the Troposphere." Science **276**: 1058.
- Russell, A. G., G. J. McRae, et al. (1983). "Mathematical Modeling of the Formation and Transport of Ammonium Nitrate Aerosol." Atmos. Environ. **17**(5): 949.
- Silva, P. J. and K. A. Prather (1997). "On-Line Characterization of Individual Particles from Automobile Emissions." Environ. Sci. and Technol. **31**: 3074.
- Vogt, R., C. Elliott, et al. (1996). "Some New Laboratory Approaches to Studying Tropospheric Heterogeneous Reactions." Atmos. Environ. **30**: 1729.

Weiss, M., P. J. T. Verheijen, et al. (1997). "On the Performance of an On-Line Time-of-Flight Mass Spectrometer for Aerosols." J. Aerosol Sci. **28**: 159.

Wood, S. H. and K. A. Prather (1998). "Time-of-Flight Mass Spectrometry Methods for Real Time Analysis of Individual Aerosol Particles." Trends in Anal. Chem. **17**: 346.

Yang, M., P. T. A. Reilly, et al. (1996). "Real-time Chemical Analysis of Aerosol Particles using an Ion Trap Mass Spectrometer." Rapid Commun. in Mass Spectrom. **10**: 347.